Slab-Triggered Arc Flare-up in the Cretaceous Median Batholith and the Growth of Lower Arc Crust, Fiordland, New Zealand

Decker, M.,[1] Schwartz, J.J.,[1*] Stowell, H.H.,[2] Klepeis, K.A.,[3] Tulloch, A.J.,[4] Kitajima, K.,[5] Valley, J.W.,[5] Kylander-Clark, A.[6]

ABSTRACT

The Mesozoic continental arc in Fiordland, New Zealand, records a ca. 110 Ma history of episodic, subduction-related magmatism that culminated in a terminal surge of mafic to intermediate, high-Sr/Y, calc-alkalic to alkali-calcic magmas. During this brief, 10-15 Ma event, more than 90% of the Cretaceous plutonic arc root was emplaced; however the source of these rocks and the degree to which they represent lower crustal mafic and/or metasedimentary recycling versus the addition of new lower arc crust remains uncertain. We report whole-rock geochemistry and zircon trace-element, O-isotope and Hf-isotope analyses from 18 samples emplaced into lower arc crust (30-60 km depth) of the Median Batholith with the goals of: a) evaluating processes that triggered the Cretaceous arc flare-up event, and b) determining the extent to which the Cretaceous arc flare up resulted in net addition of lower arc crust. We find that $\delta^{18}O$ (Zrn) values from the Western Fiordland Orthogneiss ranges from 5.2 to 6.3‰ and yields an error-weighted average value of 5.74 ± 0.04‰ (2SE, 95% confidence limit). LA-MC-ICPMS results yield initial εHf (Zrn) values ranging from -2.0 to +11.2 and an error-weighted

[1] Department of Geology, California State University Northridge, CA, 91330, USA
[2] Department of Geological Sciences, The University of Alabama, AL 35487, USA
[3] Department of Geology, The University of Vermont, VT, 05405, USA
[4] GNS Science, Private Bag 1930, Dunedin, NZ
[5]WiscSIMS, Dept. of Geoscience, University of Wisconsin, Madison, WI 53706, USA
[6] Department of Earth Science, University of California Santa Barbara, Santa Barbara, CA, 93106, USA
[*] corresponding author: email: joshua.schwartz@csun.edu; tel. (401) 742-2583

average value of +4.2 ± 0.2. We explore the apparent decoupling of O- and Hf-isotope systems through a variety of mass-balance mixing and assimilation-fractional crystallization models involving depleted- and enriched-mantle sources mixed with supra-crustal contributions. We find that the best fit to our isotope data involves mixing between an enriched, mantle-like source and up to 15% subducted, metasedimentary rocks. These results together with the homogeneity of $\delta^{18}O$ (Zrn) values, the high-Sr/Y signature, and the mafic character of Western Fiordland Orthogneiss magmas indicate that the Cretaceous flare-up was triggered by partial melting and hybridization of subducted oceanic crust and enriched subcontinental lithospheric mantle. We argue that the driving mechanism for the terminal magmatic surge was the propagation of a discontinuous slab tear beneath the arc, or a ridge-trench collision event, at ca. 136-128 Ma. Our results from the Early Cretaceous Zealandia arc contrast with the strong crustal signatures that characterize high-flux magmatic events in most shallow to mid-crustal, circum-Pacific orogenic belts in the North and South American Cordillera and the Australia Tasmanides; instead, our results document the rapid addition of new lower arc crust in <<15 m.y. with lower crustal growth rates averaging 40-50 km^3/Ma/arc-km from 128-114 Ma, and peaking at 150-210 km^3/Ma/arc-km from 118-114 Ma when ~70% of the arc root was emplaced. Our results highlight the significant role of Cordilleran arc flare-up events in the rapid, net generation of continental crust through time.

Keywords: arc flare up, lower arc crust, zircon, oxygen isotopes, Hf isotopes, high Sr/Y melts

INTRODUCTION

Continental arcs are often considered factories of crustal growth whereby partial melting of mantle adds to the growth of the evolving continental crust (Tatsumi and Stern, 2006; Scholl and von Huene, 2007; 2009; Hawkesworth et al., 2010; Voice et al., 2011). In circum-Pacific orogens, the long-term (>100 m.y.) magmatic evolution of continental arcs is dominated by mantle-derived magmatism (Collins et al., 2011); however, the pace of magmatism in arcs has long been recognized to be non-steady state, characterized by episodic periods of high-volume magmatic pulses, termed high magma addition rate (MAR) events, that occur within a background of lower-volume activity (Armstrong, 1988). These high-MAR events represent short-term (<20 m.y.) excursions from long-term magmatic trends, yet they overwhelmingly dominate arc magma addition rates (Scholl and von Huene, 2007; Ducea and Barton, 2007; Ducea et al., 2015a; Paterson et al., 2015; Ducea et al., 2017). Their cause(s) and the degree to which they contribute to the net addition of new continental crust are fundamental and yet unresolved problems in understanding geodynamic controls on continental crustal growth through time.

In well-studied Phanerozoic continental arcs, geochemical and isotopic data suggest that high-MAR events involve significant reworking of pre-existing crust, and evidence for significant volumes of mantle-derived melts is often conspicuously absent (e.g., Ducea, 2001; Saleeby et al., 2003; Lackey et al., 2005; Ducea and Barton, 2007; Paterson et al., 2011; Ducea et al., 2015a; Paterson et al., 2015). This problem is underscored in various circum-Pacific arc segments of the North and South American Cordilleran and the Australian Tasmanides where high-MAR events are particularly well documented. For example, in the eastern Peninsular Ranges batholith, voluminous tonalitic to granodioritic magmas of the La Posta Pluton (94-91 Ma) display elevated $\delta^{18}O$ values (9-12.8‰) and radiogenic isotope signatures that reflect significant contributions from ancient crustal sources (Taylor and Silver, 1978; Silver et al., 1979; Kistler et al., 2014). In other shallow- to mid-crustal batholiths, such as the Cretaceous Sierra Nevada batholith, geochemical and isotopic studies demonstrate that ~50% or more of the magmatic budget was derived from pre-existing, upper-plate crustal material (Ducea, 2001; Lee et al., 2006; Ducea and Barton, 2007; Lackey et al., 2008; Lackey et al., 2012; Ducea et al., 2015b). On the opposite side of the Pacific basin in the Australian Tasmanides, repeated arc retreat followed by closure of oceanic back-arc basins produced wide-spread melting of craton-derived turbiditic metasedimentary rocks and the generation of 'classic' S-type granites (Kemp et al., 2009). Taken as a whole, geochemical and isotopic patterns from large portions of circum-Pacific magmatic belts reveal complex tectonic reorganizations through time and the reworking of pre-batholithic basement and supra-crustal rocks in the generation and modification of arc crust during voluminous magmatic surges (e.g., Ducea and Barton, 2007; Lackey et al., 2008; DeCelles et al., 2009; Chapman et al., 2013).

A key problem in understanding crustal growth processes in circum-Pacific magmatic belts is that much of our information is dominated by studies of shallow to mid-crustal plutons that may have undergone significant assimilation of wall rocks during ascent through the crustal column, and/or hybridization of original mantle-derived magmas at depth in lower crustal melting, assimilation, storage and homogenization zones (Hildreth and Moorbath, 1988). This problem is particularly acute in over-thickened continental arcs where the crustal column may reach 70-75 km (Beck et al., 1996). The involvement of mantle-derived melts in high-MAR events has long been noted in whole rock and mineral isotopic data (Cui and Russell, 1995; Kemp et al., 2007; Kemp et al. 2009; Appleby et al., 2010; Shea et al., 2016); however, the significance of mantle processes in triggering high-MAR events remains controversial in part due to a lack of exposure of deep portions of the crust generated during voluminous arc magmatism (Ducea, 2001; de Silva et al., 2015; Paterson and Ducea, 2015; Ducea et al., 2017).

Here, we investigate a deep-crustal flare-up along the Mesozoic, paleo-Pacific margin of southeast Gondwana, now isolated and preserved in the largely submerged continent 'Zealandia' (Mortimer et al. 2017) with the goals of: a) evaluating processes that triggered the voluminous surge of mafic to intermediate magmatism, and b) determining the extent to which the Cretaceous arc flare up resulted in the addition of new lower continental crust. We focus on the western Fiordland sector of the Mesozoic Median Batholith (Fig. 1) because it exposes a section of lower continental arc crust (1.0 to 1.8 GPa, or 35 to 65 km paleo-depth: Allibone et al., 2009a,b; De Paoli et al., 2009) generated in a high-flux magmatic episode during which the entire Mesozoic plutonic arc root was emplaced in ~14 m.y. from 128 to 114 Ma (Schwartz et al., 2017). This unique lower crustal exposure allows us to investigate the geochemical and isotopic composition of the lower arc rocks that have not been significantly modified by transport through the crustal column during ascent.

Results from our study indicate that $\delta^{18}O$ (Zrn) values from the Cretaceous arc root give uniformly mantle-like values ranging from 5.2 to 6.3‰ and yield an error-weighted average value of 5.74 ± 0.04‰ (2SE; n=126). These results indicate that the surge of lower crustal arc magmas was primarily sourced from the underlying mantle with only limited contributions from upper plate materials. We present a model whereby the arc flare-up was triggered by widespread partial melting of a metasomatized, subcontinental lithospheric mantle with contributions from partially melted, subducted eclogite-facies metasedimentary rocks and oceanic crust. Our isotopic results reveal that the terminal Cretaceous flare-up resulted in the rapid addition of new continental crust to the base of the Median Batholith in <<15 m.y. with crustal production rates averaging ~40-50 km^3/Ma/arc-km from 128-114 Ma, and peaking at ~150-210 km^3/Ma/arc-km from 118-114 Ma.

GEOLOGIC FRAMEWORK

The Median Batholith in Fiordland

The Median Batholith outcrops over 10,000 km^2 and is located within the Western Province of New Zealand (Mortimer et al., 1999; Tulloch and Kimbrough, 2003; Mortimer et al., 2014). It consists of two margin-parallel plutonic belts, which are compositionally distinct: an older, low-Sr/Y (<40), outboard arc located primarily in eastern Fiordland, and an inboard plutonic belt of high-Sr/Y character (>40) located primarily in central and western Fiordland. Collectively, these belts preserve a record of episodic magmatism active over >150 Ma along the southeastern Gondwana margin from 260-114 Ma. Arc magmatism resulted in at least two recognized surges of low- and high-Sr/Y magmas at ca. 147-136 Ma and 128-114 Ma, respectively, both of which occurred over ca. 10-15 Ma each (Schwartz et al., 2017). The latter surge of magmatism resulted in emplacement of the Separation Point Suite (SPS) shortly before termination of arc magmatism and the initiation of extensional orogenic collapse beginning at 108-106 Ma (Schwartz et al., 2016). The boundary between the inboard and outboard arcs is marked by the Grebe Mylonite zone (Fig. 1) (Allibone et al., 2009a; Scott et al., 2009; Scott et al., 2011; Scott, 2013) and other major subvertical contractional to transpressional shear zones (Klepeis et al., 2004; Marcotte et al., 2005).

Outboard arc

The primary Mesozoic component of the outboard arc is the low-Sr/Y Darran Suite (Muir et al., 1995; Tulloch and Kimbrough, 2003). Darran Suite magmatism occurred on or near the paleo-Pacific margin of southern Gondwana from 230-136 Ma with peak magmatic activity taking place between 147-136 Ma (Kimbrough et al., 1994; Muir et al., 1998; Schwartz et al., 2017 and references therein). It is characterized by mafic and felsic (gabbroic to granitic) I-type plutonic rocks likely derived from mantle wedge melting and/or mafic sources (Muir et al., 1998). Whole rock $\delta^{18}O$ values in the Darran Suite range from 4.6 to 5.4‰ with an average value of 5.03‰ (n=12; Blattner and Williams, 1991). Decker (2016) reported that some Darran Suite rocks emplaced from 169-135 Ma have low $\delta^{18}O$ (Zrn) values ranging from 3.8 to 4.9‰. The Early Cretaceous Largs Group volcanic rocks located in NE Fiordland also display anomalously low whole rock (WR) $\delta^{18}O$ values ranging from +3.3 to -12.3‰ (n=26) indicating hydrothermal alteration by meteoric fluids at high latitudes or high paleo-elevations (Blattner and Williams, 1991; Blattner et al., 1997). Initial Hf isotope (Zrn) values from Darran Suite plutons give values ranging from +8 to +11 (Scott et al., 2011; Decker, 2016). Whole rock initial εNd values range from +3 to +4 (Muir et al., 1998), and initial $^{87}Sr/^{86}Sr$ ratios range from ca. 0.7037 to 0.7049.

Darran Suite magmatism terminated at ca. 136 Ma and was followed by the emplacement of high-Sr/Y tonalites and granodiorites of the SPS from 128 to 105 Ma at depths of approximately 0.2-0.7 GPa (Muir et al. 1995; 1998; Tulloch and Challis, 2000; Tulloch and Kimbrough, 2003; Allibone and Tulloch, 2004: 2008; Bolhar et al., 2008). Although the SPS plutonic belt mostly lies inboard of the Darran Suite plutonic belt, intrusions into the outboard Darran Suite are also common and have been extensively studied (Muir et al., 1998; Tulloch and Kimbrough, 2003; Bolhar et al., 2008). Both Darran and SPS plutonic suites are calc-alkalic to alkali-calcic in composition (Tulloch and Kimbrough, 2003). Muir et al. (1998) report that SPS plutons display a small range of positive, whole rock initial εNd values of ca. +3, and low $^{87}Sr/^{86}Sr$ initial ratios of ca. 0.7038. Bolhar et al. (2008) report initial εHf (Zrn) values ranging from +8.1 to +11.8 from the same plutonic rocks east of the Grebe Mylonite Zone. Zircon $\delta^{18}O$ values for the same rocks range from 1.0 to 5.2‰. They argue that SPS magmas east of the Grebe Mylonite zone were primarily sourced from remelted mafic arc crust (e.g., Darran Suite rocks) and assimilated small amounts of hydrothermally altered, low $\delta^{18}O$ crust at the level of emplacement.

Inboard arc, including the Separation Point Suite

Mesozoic magmatism in the inboard belt is dominated by Cretaceous SPS and related plutons (Muir et al. 1995; 1998; Tulloch et al., 2003). Tonalites and granodiorites west of the Grebe Mylonite zone occur in central and southwestern Fiordland and give zircon crystallization dates ranging from 120.8 to 116.3 Ma (Scott and Palin, 2008; Ramezani and Tulloch, 2009). No isotopic data are reported from tonalitic to granodioritic rocks west of the Grebe Mylonite zone.

In western Fiordland, deep-crustal plutons of the SPS were emplaced at 1.0-1.8 GPa and formed the Western Fiordland Orthogneiss (Allibone et al., 2009a,b; DePaoli et al., 2009). These lower crustal rocks are the focus of this study and include seven major plutons: Worsley, McKerr Intrusives (Western and Eastern), Misty, Malaspina, Breaksea Orthogneiss, and Resolution Orthogneiss. Plutonic rocks are primarily diorites and monzodiorites and locally intruded the Deep Cove Gneiss at 128-114 Ma (Mattinson et al., 1986; Tulloch and Kimbrough 2003; Hollis et al., 2003; Allibone et al., 2009a; Schwartz et al., 2017). The Deep Cove Gneiss is a heterogeneous unit chiefly consisting of quartzofeldspathic paragneiss, marble, calc-silicate, and hornblende-plagioclase gneiss (Oliver, 1980; Gibson, 1982). Emplacement of the Western

Fiordland Orthogneiss was synchronous with regional transpression/contractional deformation in northern Fiordland (Pembroke Valley and Mt. Daniel) and in the Caswell Sound fold-and-thrust belt in western Fiordland (Daczko et al., 2001; 2002; Klepeis et al., 2004; Marcotte et al., 2005). Subsequent granulite- to upper amphibolite-facies metamorphism occurred from 116 to 102 Ma and overlapped with the initiation of extensional orogenic collapse in the deep crust at 108-106 Ma (Hollis et al., 2003; Flowers et al., 2005; Stowell et al., 2014; Klepeis et al., 2016; Schwartz et al., 2016). For deformation and metamorphic descriptions of the Western Fiordland Orthogneiss see: Oliver (1976, 1977), Gibson & Ireland (1995), Clarke et al. (2000), Daczko et al. (2002), Hollis et al. (2004), and Klepeis et al. (2004, 2007), Allibone et al. (2009b), Stowell et al. (2014), and Klepeis et al. (2016).

Plutonic rocks from the Western Fiordland Orthogneiss are characterized by low SiO_2 (<50-60 wt.%), Y (<20 ppm) and HREE concentrations (Yb< 2.0 ppm); and high Al_2O_3 (>18 wt.%), Na_2O (4.0 wt.%), Sr (>1000 ppm), and Sr/Y and La/Yb values (>50 and >15, respectively) (McCulloch et al., 1987). They display steeply fractionated LREE/HREE ratios and lack positive or negative europium anomalies. Relative to NMORB, they display LILE enrichment with pronounced positive Pb and Sr anomalies, and negative Rb, Nb and sometimes Zr anomalies (McCulloch et al., 1987). Isotopically, they display weak enrichment in $^{87}Sr/^{86}Sr$ initial ratios of 0.70380 to 0.70430, and weakly negative to positive εNd values ranging from -0.4 to +2.7 to (McCulloch et al., 1987; Muir et al., 1998). Geochemical modeling of Western Fiordland Orthogneiss magmas from the Malaspina Pluton demonstrate that the variation in major-element chemistry reflects fractional crystallization of low silica phases including garnet, clinopyroxene and plagioclase (Chapman et al., 2016). Although Western Fiordland Orthogneiss plutonic rocks bear strong similarities to high-Sr/Y granitic plutons in eastern and central

Fiordland, their low SiO_2 concentrations and more evolved radiogenic isotope values distinguish them from their shallower level counterparts. Similar composition lavas are commonly known as adakites, and Archean analogues are referred to as tonalite-trondhjemite-granodiorites (TTGs) (see comprehensive review in Moyen, 2009). However, we prefer the term 'high-Sr/Y plutonic rocks' to describe the Western Fiordland Orthogneiss as the term avoids genetic connotations (see discussion in Tulloch and Kimbrough, 2003). Western Fiordland Orthogneiss plutonic rocks bear strong similarities to a subclass of high-Sr/Y rocks termed "low-silica adakites" (Martin et al., 2005) that are commonly interpreted to have formed from interactions between slab melts and peridotitic mantle (e.g., Rapp et al., 1999; Kelemen et al. 2003; Kelemen et al. 2014). We return to this idea and the petrogenesis of the Western Fiordland Orthogneiss in the discussion section.

METHODS

Whole-rock geochemistry

Whole-rock samples were powdered in an alumina ceramic shatter box and major and trace-element analyses were conducted at Pomona College. Oxygen isotope analyses were conducted at the University of Wisconsin-Madison by laser fluorination as described by Valley et al. (1995) and Spicuzza et al. (1998a,b). All $\delta^{18}O$ values are reported relative to Vienna Standard Mean Ocean Water (VSMOW).

Zircon trace-element geochemistry

Zircon trace-element geochemical data were collected simultaneously with U-Pb isotopes, and age data for these zircons are reported in Schwartz et al. (2017). Detailed descriptions of methods are given in the Appendix, and sample locations are provided in Appendix Table 1. Analyses for U-Pb and trace elements were performed on the SHRIMP-RG ion microprobe at the USGS-Stanford laboratory utilizing an O^{2-} primary ion beam, varying in intensity from 4.3 to 6.4 nA, which produced secondary ions from the target that were accelerated at 10 kV. The analytical spot diameter was between ~15-20 microns and a depth of 1-2 microns for each analysis performed in this study. Prior to every analysis, the sample surface was cleaned by rastering the primary beam for 60-120 seconds, and the primary and secondary beams were auto-tuned to maximize transmission. The duration of this procedure typically required 2.5 minutes prior to data collection. The acquisition routine included $^{89}Y+$, 9-REE ($^{139}La+$, $^{140}Ce+$, $^{146}Nd+$, $^{147}Sm+$, $^{153}Eu+$, $^{155}Gd+$, $^{163}Dy^{16}O+$, $^{166}Er^{16}O+$, $^{172}Yb^{16}O+$), a high mass normalizing species ($^{90}Zr_2{}^{16}O+$), followed by $^{180}Hf^{16}O+$, $^{204}Pb+$, a background measured at 0.045 mass units above the $^{204}Pb+$ peak, $^{206}Pb+$, $^{207}Pb+$, $^{208}Pb+$, $^{232}Th+$, $^{238}U+$, $^{232}Th^{16}O+$, and $^{238}U^{16}O+$. Measurements were made at mass resolutions of M/ΔM = 8100-8400 (10% peak height), which eliminated interfering molecular species, particularly for the REE. For some samples, the analysis routine was the same as above, but also included masses $^{30}Si^{16}O+$, $^{48}Ti+$, $^{49}Ti+$, and $^{56}Fe+$. Measurements for these samples were performed at a mass resolutions of M/ΔM = 9000-9500, which was required to fully separate the $^{48}Ti+$ peak from the nearby $^{96}Zr++$ peak. Analyses consisted of 5 peak-hopping cycles stepped sequentially through the run table. The duration of each measurement ranged between 15-25 minutes on average. Count times for most elements were between 1-8 seconds, with increased count times ranging from 15-30 seconds for ^{204}Pb, ^{206}Pb, ^{207}Pb, and ^{208}Pb to improve counting statistics and age precision. Similar to previous studies, U concentrations were quite low (roughly <200 ppm) for zircons from mafic to intermediate composition rocks. Zircon standard, R33, was analyzed after every 3-5 unknown zircons. Average count rates of each element were ratioed to the appropriate high mass normalizing species to account for any primary current drift, and the derived ratios for the unknowns were compared to an average of those for the standards to determine concentrations. Spot-to-spot precisions (as measured on the standards) varied according to elemental ionization efficiency and concentration.

For the zircon standards MAD-green (4196 ppm U, Barth and Wooden, 2010) and MADDER (3435 ppm U), precision generally ranged from about ±3% for Hf, ±5-10% for the Y and HREE, typically ±10-15%, but up to ±40% for La, which was present most often at the ppb level (all values at 2σ). Trace elements (Y, Hf, REE) were measured briefly (typically 1 to 3 sec/mass) immediately before the geochronology peaks in mass order. All peaks were measured on a single EPT® discrete-dynode electron multiplier operated in pulse counting mode. Analyses were performed using 5 scans (peak-hopping cycles from mass 46 through 254), and counting times on each peak were varied according to the sample age as well as the U and Th concentrations in order to improve counting statistics and age precision. Chondrite normalized plots were calculated using values from McDonough & Sun (1995).

Zircon Secondary Ion Mass Spectrometry O isotopes

Zircon oxygen isotope analyses were conducted at the University of Wisconsin-Madison using the CAMECA IMS 1280 ion microprobe following the procedures outlined in Kita et al. (2009) and Valley and Kita (2009). All mounts were polished using 6, 3, and 1μm diamond lapping film to expose the surface of the zircons just below the bottom of the existing pits from U-Pb SHRIMP-RG analysis. Where U-Pb pits were visible after polishing, they were avoided so that O-implantation from SHRIMP-RG analyses did not affect oxygen isotope ratios. Zircons were imaged by reflected light and by SEM-cathodoluminescence at CSUN to aid in the selection of oxygen isotope analysis spot locations. Mounts were cleaned using a series of ethanol and deionized water baths in an ultrasonic cleaner, then dried in a vacuum oven at ~40 °C for 1 hour, and gold-coated in preparation for SIMS analysis. Zircon mounts were mounted with the KIM-5 oxygen isotope standard (Valley 2003, $\delta^{18}O$ = 5.09‰ VSMOW). Extra care was taken to achieve a smooth, flat, low relief polish. A focused, 10kV $^{133}Cs^{+}$ primary beam was used for analysis at 1.9-2.2 nA and a corresponding spot size of 10-12 μm. A normal incident electron gun was used for charge compensation. The secondary ion acceleration voltage was set at 10kV and oxygen isotopes were collected in two Faraday cups simultaneously with $^{16}O^{1}H$. Ratios of OH/O provide a monitor of "water", which can identify domains of metamict zircon or inclusions (Wang et al. 2014). Four consecutive measurements of zircon standard KIM-5 were analyzed at the beginning and end of each session, and every 8-10 unknowns throughout each session. The average values of the standard analyses that bracket each set of unknowns were used to correct for instrumental bias. The average precision (reproducibility) of the bracketing standards for this study ranged from ± 0.12 to ± 0.44 and averaged ± 0.28‰ (2SD). After the oxygen isotope analysis was complete, ion microprobe pits were re-imaged by the SEM at CSUN to ensure that there were no irregular pits or inclusions.

Zircon LA-MC-ICPMS Lu-Hf Isotopes

Hafnium isotopes were analyzed via laser ablation at the University of California Santa Barbara using a MC-ICP-MS (multicollector –inductively coupled plasma-mass spectrometer) in an analytical session on August 6 and 7, 2015. Whenever possible, O-isotope spot locations were resampled for Hf isotopes to target the same chemical domain. Mounts were polished between

U-Pb, O, and Hf analysis such that the original U-Pb spot was no longer visible. Careful documentation of the CL images allowed for accurate placement of spots during analysis. A 50μm beam diameter, 3.5 mJ energy (approximately 80 nm per pulse), and a 10 Hz repetition rate were used for all ablations. Analyses were conducted over a 30 second ablation period with a 45 second washout between measurements. Masses 171-180 (Yb, Hf, Lu) were measured simultaneously on an array of 10 Faraday cups at 1-amu spacing. Data reduction was preformed using Iolite 2.3 (Paton et al., 2011).

The MC-ICP-MS is not able to differentiate between ^{176}Yb, ^{176}Lu, and ^{176}Hf, therefore, the ^{176}Hf intensity must be corrected for isobaric interferences. Natural ^{173}Yb/^{171}Yb=1.123575 was used to calculate the Yb mass bias factor and and Lu mass bias (Thirlwall and Anczkiewicz 2004), and ^{179}Hf/^{177}Hf= 0.7325 was used to calculate the Hf mass bias (Patchett and Tatsumoto 1980; Vervoort et al., 2004). ^{176}Yb/^{173}Yb=0.786847 and ^{176}Lu/^{175}Lu=0.02656 were used to subtract isobaric interferences on ^{176}Hf (Patchett and Tatsumoto 1980; Thirlwall and Anczkiewicz 2004; Vervoort et al., 2004). A variety of zircon hafnium standards with known hafnium compositions were analyzed before and after ~10 unknowns, and yield weighted averages within uncertainty of their accepted values (see Appendix file).

RESULTS

Sample descriptions

Geochemical data consist of 56 new whole-rock samples collected from >2300 km^2 of lower crust in Western Fiordland (Fig. 2). Our data span ~130 km parallel and ~30 km perpendicular to the strike of the paleo-arc axis, which is roughly approximated by the present-day western Fiordland coastline. Samples for isotopic analysis consist of a subset and include eight samples from the Misty Pluton, five samples from the Malaspina Pluton, two samples from the Worsley Pluton, one sample from the Resolution Orthogneiss, one sample from the Breaksea Orthogneiss, and one sample from the Eastern McKerr Intrusives (Fig. 1). Oxygen and Hf isotope measurements were conducted on the same chemical domain as U-Pb isotope determinations where possible (see Fig. 3). Zircon trace element, $\delta^{18}O$ and initial εHf isotope values are shown in Figs. 4-9.

Whole-rock geochemical data

Rocks from the Western Fiordland Orthogneiss range in composition from trachy-basalts to trachy-andesites (Fig. 2A). They are magnesian, calc-alkalic to alkali-calcic, and metaluminous (Fig. 2B-D), similar to plutonic rocks in other Cordilleran plutons and batholiths (Frost et al., 2001). Molar Mg#s range from 56 to 43, and display fractional crystallization trends consistent with removal of high-pressure mineral assemblages including clinopyroxene + garnet (Chapman et al., 2016). All plutonic rocks from the Western Fiordland Orthogneiss display high average Al_2O_3 (18.6 wt.%), Na_2O (4.9 wt.%), Ni (26 ppm), Cr (83 ppm), Sr (1300 ppm), Sr/Y values (128), and low average Y (14 ppm) and heavy rare earth element concentrations (Yb=1.4 ppm) (n=175). Compared to NMORB, plutonic rocks have pronounced positive Ba, K, Pb, and Sr anomalies, and negative Nb and Zr anomalies. Measured $\delta^{18}O$ (WR) ranges from 5.3 to 6.8‰, with one sample as low as 4.5‰ (13NZ22). The mean value of all $\delta^{18}O$ (WR) values (excluding the outlier) is 6.0 ± 0.4‰ (Table 1).

Zircon trace-element geochemistry

Zircons from the Western Fiordland Orthogneiss are distinguished from continental arc and mid ocean ridge (MOR) zircons by strongly enriched U/Yb values at low Hf concentrations (Fig. 4A). Misty Pluton zircons show the highest Hf concentrations of all zircons. Western Fiordland Orthogneiss zircons are also characterized by high Gd/Yb and low Yb values reflecting strongly fractionated middle/heavy rare earth element concentrations and depletions in heavy rare earth element concentrations (Fig. 4B-E). Western Fiordland Orthogneiss zircons are also characterized by high Ti concentrations, which reflect high average crystallization temperatures using the Ferry and Watson (2007) calibration (typically >750°C assuming $a_{SiO2}=1$ and $a_{TiO2}=0.6$; see Schwartz et al., 2017 for zircon-thermometry details) (Fig. 4D-E). Western Fiordland Orthogneiss zircons also display enrichments in Ce/Yb (Fig. 4C). Using the calibration in Trail et al. (2011), Ce/Ce* values from Western Fiordland Orthogneiss zircon data give an average fO_2 of ~5.0 log units above the value defined by the fayalite-magnetite-quartz (FMQ) buffer (±3.2 log units).

Zircon oxygen isotope ratios

Individual zircon $\delta^{18}O$ values in the Western Fiordland Orthogneiss range from 5.2 to 6.3‰ (Table 1; Supplementary file). The mean value of all zircons is 5.76 ± 0.46‰ (2SD), and the error-weighted average is 5.74 ± 0.04‰ (2SE, 95% confidence limit) (Fig. 5A). In samples where we measured internal and external domains, we see no measurable difference in $\delta^{18}O$ values (e.g., 15NZ27: Fig. 3). Within individual samples, measured values tightly cluster and yield standard deviations ranging from 0.08 to 0.59‰ (2SD). Intra-pluton $\delta^{18}O$ standard deviations are also small, <0.6‰. From north to south, mean intra-pluton values and 2SD are: 5.73 ± 0.59‰ (Worsley Pluton), 5.77 ± 0.35‰ (Eastern McKerr Intrusives), 5.82 ± 0.39‰

(Misty Pluton), 5.73 ± 0.29‰ (Malaspina Pluton), 5.85 ± 0.59‰ (Resolution Orthogneiss), and 5.30 ± 0.59‰ (Breaksea Orthogneiss). All individual zircons and mean intra-pluton values for the Western Fiordland Orthogneiss lie within analytical SIMS error of the high-temperature mantle value for zircon (5.3 ± 0.80‰: 2SD; Valley, 2003). There are no temporal or latitudinal trends in $\delta^{18}O$ (Zrn) values (Fig. 6A-B).

Calculated WR values from measured $\delta^{18}O$ (Zrn) using the equation of Lackey et al. (2008) generally agree with measured $\delta^{18}O$ whole rock; however, several samples display deviations towards lower $\delta^{18}O$ (WR) values. (Fig. 7; Table 1). Samples with the largest deviations include two samples from the Malaspina Pluton (13NZ22, which also has the lowest $\delta^{18}O$ (WR) value, and 13NZ16B), the two Worsley Pluton samples (15NZ02, and 15NZ27), and one sample from the Misty Pluton (12NZ36b).

Zircon Lu-Hf isotopes

Initial epsilon hafnium values in the Western Fiordland Orthogneiss range from -2.0 to +11.3, and the error-weighted average for all zircons is +4.2 ± 0.2 (MSWD = 0.6; n = 354) (Fig. 5B). From north to south, weighted average initial εHf values for plutons are: +5.0 ± 0.5 for the Worsley Pluton (MSWD = 0.3; n = 40), +3.8 ± 0.7 for the Eastern McKerr Intrusives (MSWD = 1.1; n = 20), +4.2 ± 0.2 for the Misty Pluton (MSWD = 0.5; n = 160), +3.9 ± 0.3 for the Malaspina Pluton (MSWD = 0.6; n = 94), +3.9 ± 0.7 for the Resolution Orthogneiss (MSWD = 0.5; n = 20), and +4.6 ± 0.7 for the Breaksea Orthogneiss (MSWD = 0.4; n = 20). In general, Western Fiordland Orthogneiss values are significantly more evolved than Cretaceous depleted mantle (~+15), and our results overlap with existing results from the Western Fiordland Orthogneiss (Bolhar et al., 2008; Milan et al., 2016).

DISCUSSION

Zircon geochemical constraints on lower crustal magma sources

Zircons from the Western Fiordland Orthogneiss are distinguished from arc and N-MORB zircons by enrichment in U/Yb values suggesting either significant crustal input or derivation from an enriched mantle source (Fig; 4A). Mantle-like $\delta^{18}O$ values for all zircons in this study (see discussion below and Figs. 5-6) preclude significant, if any, crustal input, and implies that the source of elevated trace element values is an enriched mantle source. Strongly fractionated middle/heavy rare earth element concentrations and depletions in heavy rare earth element concentrations (Fig. 4B-C) further indicate the presence of garnet as a fractionating and/or residual phase in the source region. These features also characterize Hawaiian and Icelandic zircons. Weak trends in Ti-Yb space can be indicative of either garnet and/or late-stage amphibole crystallization (Fig 4D); however, even the most primitive zircons with the highest Ti values show strong depletions in Yb concentrations indicating that Western Fiordland Orthogneiss magmas were depleted in heavy rare earth elements, likely from residual garnet in the source region, prior to zircon crystallization.

Western Fiordland Orthogneiss also display enrichments in Ce/Yb relative to MOR, intraplate and other continental zircons (Fig. 4C), suggesting crystallization from relatively oxidizing magmas. These features are consistent with high average calculated fO_2 values (~5.0 log units above the value defined by the FMQ buffer), and petrologic observations of Bradshaw (1989, 1990) who noted that Western Fiordland Orthogneiss oxide assemblages are characterized by intergrowths of exsolved ilmenite and hematite, indicating relatively oxidizing conditions of crystallization. Collectively, zircon trace element data indicate that zircons crystallized from trace element enriched, mafic magmas that were relatively oxidizing, and depleted in heavy rare earth elements.

Zircon O and Hf isotope constraints on lower crustal magma sources

Zircons from the lower crust of the Median Batholith are characterized by uniformly low $\delta^{18}O$ values with all analyses lying within analytical SIMS error of high-temperature mantle values (Fig. 5A) indicating equilibration between Western Fiordland Orthogneiss zircons and mantle-like melts. Whole rock $\delta^{18}O$ values from the same rocks are also characterized by mantle-like values; however, several samples display evidence for modest open-system exchange after magmatic crystallization (Fig. 7; Table 1). We therefore base our interpretations primarily on $\delta^{18}O$ (Zrn), which is highly retentive of magmatic $\delta^{18}O$ even in rocks that have undergone subsolidus exchange and hydrothermal alteration (Valley, 2003; Lackey et al., 2006; Page et al., 2007; Lackey et al., 2008).

In addition to their mantle-like character, zircons display very little intra- and inter-sample variation in $\delta^{18}O$ values, consistent with the lack of measurable differences between internal and external domains (Fig. 3). This observation is remarkable given the wide geographic distribution of our samples that span >2300 km^2 of lower arc crust (Fig. 1). Together, the homogeneity of $\delta^{18}O$ (Zrn) values, the mantle-like $\delta^{18}O$ character of both zircon and whole rock, and the low SiO_2 whole rock values for Western Fiordland Orthogneiss rocks in this study (54.7 ± 2.3: 1SD) support the interpretation that Western Fiordland Orthogneiss magmas were derived from partial melting of a high-temperature mantle or mantle-like sources.

In contrast to the mantle-like $\delta^{18}O$ zircon and whole rock values, initial εHf (Zrn) values range from -2.0 to +11.2 with a mean of +4.2 (Table 1; Fig. 6B). These values are significantly lower than Cretaceous depleted MORB mantle (~15: Vervoort et al., 1999) and average modern island-arc values (~13: Dhuime et al., 2011). Since the Hf budget of crustal rocks is largely contained within zircon, contamination from pre-existing zircon-bearing sources is likely to strongly affect the distribution of Hf-isotope values. A curious feature of the Western Fiordland Orthogneiss zircons is that their strong mantle-like $\delta^{18}O$ values and lack of xenocrystic zircon cargo appear inconsistent with significant crustal contamination.

We explore possible explanations for decoupling of O- and Hf-isotopes by considering a variety of mixing and assimilation-fractional crystallization (AFC) scenarios involving wall rock, subducted metasedimentary rocks, and various depleted- and 'enriched'-mantle sources. Here we use 'enriched' to describe εHf values significantly lower than Cretaceous depleted mantle (+15). Epsilon Hf values for the assimilated wall rock were calculated from average εNd values of Takaka metasedimentary rocks in Tulloch et al. (2009) using the Vervoort et al. (1999) 'crustal' Hf-Nd relationship. The average Takaka value (εNd=-7.9) is similar to that of a metasedimentary rock reported from George Sound (εNd=-9: McCulloch et al. 1987) and either value is considered viable. Epsilon Hf values and Hf concentrations for subducted sediment were selected from average pelagic sediments reported in Vervoort et al. (1999). Hf concentrations were selected from average values of metasedimentary rocks from western Fiordland (J. Wiesenfeld and J. Schwartz, unpublished data) and average values of arc lavas from the Mariana arc reported in Tollstrup and Gill (2005).

Results of binary mixture models are illustrated in Figs. 8A-B, and AFC models are shown in Figs. 8C-D. In all scenarios, mixing and AFC scenarios involve <20% interaction with Deep Cove Gneiss (Fig. 8A and C), and <10% interaction with pelagic sediments (Figs. 8B and D). Figure 8 also illustrates two important features of our data: 1) in both mixing and AFC scenarios, no single model adequately describes the distribution of Western Fiordland Orthogneiss zircon isotope data; and 2) Western Fiordland Orthogneiss zircons show no apparent mixing trends, but instead they plot in a clustered field within the mantle array centered at εHf = +4. We also observe that models with a depleted mantle source end member (εHf=+15) fail to describe the distribution of tightly clustered Western Fiordland Orthogneiss data. Similarly, the average modern island-arc source (εHf=+13) is a poor fit in both mixing and AFC models. Models that involve an 'enriched' mantle end member (εHf +3 to +9) intersect the majority of the data; however as mentioned above, our data lack obvious evidence for mixing trends. These observations suggest that neither mixing nor AFC processes involving supra-crustal sources in the lower crust are likely the primary explanation for O and Hf enrichment in the Western Fiordland Orthogneiss; instead, Hf isotopic enrichment is a primary feature of Western Fiordland Orthogneiss, reflecting derivation of an enriched source region.

Evaluating Triggering Mechanisms for the Zealandia High-MAR Event

Zircon trace element and isotopic results from the lower crust of the Median Batholith underscore the role of an enriched mantle-like source region with limited supra-crustal interaction in the petrogenesis of the Western Fiordland Orthogneiss from 128 to 114 Ma. The mantle-like oxygen isotope signatures of the Western Fiordland Orthogneiss in particular distinguish the terminal Zealandia flare-up from other Phanerozoic flare-ups, especially those in the North and South American Cordillera where widespread partial melting and/or devolatilization of fertile crustal material is commonly invoked to explain the isotopically evolved character of magmatic rocks (e.g., Ducea, 2001; Haschke et al., 2002, 2006; Kay et al., 2005; Ducea and Barton, 2007; DeCelles et al., 2009; Ramos, 2009; Chapman et al., 2013;

Ramos et al., 2014; DeCelles and Graham, 2015). Existing whole rock Pb-isotope data also rule out triggering of the flare-up by interaction with a HIMU plume (McCoy-West et al., 2016) as Western Fiordland Orthogneiss magmas have low $^{206}Pb/^{204}Pb$ signatures that are distinct from later Cretaceous intraplate lavas (Mattinson et al., 1986). Lithospheric foundering is also unlikely as a triggering mechanism as there is no evidence for significant Jurassic or Early Cretaceous magmatism or a geochemical signature of a thick lithospheric root (e.g., high Sr/Y, low heavy rare earth element concentrations) in western Fiordland prior to the Cretaceous flare-up.

In considering other possible triggering mechanisms, we note that petrologic models must address both the high-Sr/Y and calc-alkaline signature of the Western Fiordland Orthogneiss (Fig. 2). High-Sr/Y values and low heavy rare earth element concentrations, particularly Yb and Lu in Western Fiordland Orthogneiss whole rock and zircons are characteristic features and signify the presence of garnet in the source or as a fractionating phase (McCulloch et al. 1987; Muir et al. 1998; Chapman et al. 2016). In contrast, calc-alkaline signatures reflect melting of a mantle source that was previously enriched in LILEs by a hydrous fluid phase or a melt in equilibrium with garnet (Kelemen et al., 2003; 2014). In order to explain both of these features, we consider two potential scenarios including: 1) partial melting of an amphibole-rich lower crust (Muir et al. 1995; 1998; Tulloch and Kimbrough, 2003), and/or 2) partial melting and hybridization of eclogite-facies metasedimentary rocks and basalt from a subducting slab with mantle-derived melts from the subcontinental lithospheric mantle.

Before considering these petrologic scenarios, we note that the brief surge of magmatism from 128-114 Ma was linked to distinctive tectonic and magmatic features that provide insights into the geodynamic setting during the flare-up event. These features including: a) transpression and regional thrusting from ca. 130-105 Ma (Daczko et al., 2001; 2002; Marcotte et al., 2005;

Klepeis et al., 2004; Allibone and Tulloch, 2008), b) crustal thickening and possibly loading of the Western Fiordland Orthogneiss in Northern Fiordland from 128-116 Ma (Brown, 1996; Scott et al., 2009; 2011), c) a transition from dominantly low-Sr/Y magmatism from 230-136 Ma to voluminous, high-Sr/Y magmatism at 128-114 Ma (Mattinson, 1986; Muir et al., 1998; Tulloch and Kimbrough, 2003; Hollis et al., 2004; Bolhar et al., 2008; Scott and Palin, 2008; Schwartz et al., 2016), d) an apparent gap in magmatism from 136-128 Ma (Tulloch and Kimbrough, 2003; Tulloch et al. 2011), e) the initiation of early granulite facies metamorphism synchronous with magmatism at ca. 134 Ma, peaking at ca. 120-112 Ma (Gibson and Ireland, 1995; Hollis et al., 2004; Flowers et al., 2005; Stowell et al., 2010; Tulloch et al., 2011; Stowell et al., 2014; Klepeis et al., 2016; Schwartz et al., 2016); f) migration of magmatism towards Gondwana (Tulloch and Kimbrough, 2003), and g) northward drift of the Pacific Plate relative to Gondwana during the Aptian (125-112 Ma) (Davy et al. 2008). These features collectively point to a major transition in subduction zone dynamics along the southeast Gondwana margin during the interval from 136 to 128 Ma, which preceded extensional orogenic collapse of Zealandia starting at 108-106 Ma. Below we explore possible petrologic and geodynamic scenarios that may explain these features and our geochemical and isotopic data.

Partial melting of mafic lower crust

McCulloch et al. (1987) and Muir et al. (1995, 1998) proposed that the Cretaceous surge of high-Sr/Y magmas in the Western Fiordland Orthogneiss and SPS resulted from partial melting of basaltic lower crust leaving behind an eclogite to garnet amphibolite root. In the McCulloch et al. (1987) model (later refined by Tulloch and Kimbrough, 2003), the Western Fiordland Orthogneiss originated from partial melting of a LREE-enriched, low-Rb/Sr, mid- to late-Paleozoic crustal protolith equivalent to the Darran Leucogranite (SiO_2 = 51.0-53.6 wt.%). Muir et al. (1995, 1998) presented a similar model in which trenchward-directed, retroarc underthrusting of a putative backarc beneath the arc triggered widespread partial melting of mafic crust resulting in the surge of Separation Point Suite magmatism. Geologic mapping of western Fiordland has not identified either mid- to late-Paleozoic Darran Suite rocks or remnants of a mafic back-arc basin beneath the Western Fiordland Orthogneiss. Instead, the deepest portions of the arc root consist of complexly interlayered granulite facies metadiorite and eclogite, the latter of which are interpreted to represent high-pressure magmatic cumulates produced by fractional crystallization of the Western Fiordland Orthogneiss (DePaoli et al. 2009; Chapman et al. 2016).

Existing petrologic models involving melting of mafic crust also have considerable difficulty in reproducing the geochemical and isotopic features of the Western Fiordland Orthogneiss. Data from this study and data compiled from the literature (Fig. 2A) show that SiO_2 values extend to as low as 47.2 wt.%. These low values cannot be attributed to partial melting of amphibole-rich source rocks at reasonable partial melting percentages, which would produce high SiO_2 (55 to >70 wt.%) and low Mg# (20-45) melts at reasonable partial melting values (e.g., 10-30%: Rapp and Watson, 1995). Figure 2F illustrates this point by comparing melts derived from partial melting of mafic crust (grey field labeled 'slab melts') with the distribution of Western Fiordland Orthogneiss data. Note that Western Fiordland Orthogneiss data show decreasing Sr/Y with decreasing Mg# (purple line) indicating likely fractionation of both a high MgO and heavy rare earth element enriched phase. Mass balance numerical simulations of elemental data show that the diversity in Western Fiordland Orthogneiss compositions can be successfully modeled by fractionation of assemblages involving garnet + clinopyroxene from a basaltic to trachy-basaltic parental magma (Fig. 2A, E) (Chapman et al., 2016). Layered igneous garnet pyroxenites at the base of the Western Fiordland Orthogneiss in the Breaksea Orthogneiss are likely cumulates generated by this process and provide strong support for the existence of an extensive ultramafic arc root beneath the Western Fiordland Orthogneiss consistent with observed high seismic velocities (V_p >7.5 km s^{-1}) (Eberhart-Phillips and Reyners, 2001). Isotopic data from the Darran Leucogranite also preclude it as a source for the Western Fiordland Orthogneiss as it is characterized by low $\delta^{18}O$ (Zrn) values of 3.97 ± 0.32‰, and radiogenic initial εHf (Zrn) values of 8.4 ± 3.1 (2SD; Decker, 2016) that are unlike the Western Fiordland Orthogneiss. Thus, geochemical and isotopic considerations appear to rule out melting of underthrusted mafic rocks as the primary source for the Western Fiordland Orthogneiss.

Further, experimental studies also present difficulties in producing the large volumes of mafic to intermediate magmas over the timescales that we observe in the Western Fiordland Orthogneiss. Clemens and Vielzeuf (1987) demonstrated that fluid-undersaturated melting of amphibolites yields relatively low-melt volumes compared to melting of pelites and quartzofeldspathic rocks, and melt volumes decrease with increasing depth. Melt volumes are also strongly dependent on the fertility of the source rock, which is controlled by the modal abundance of hydrous phases (e.g., muscovite, biotite and amphibole). In lower arc crust, voluminous andesitic melts are unlikely to be generated by melting of underplated basaltic source rocks unless they experienced low-grade, fluid-present metamorphism resulting in a significant modal increase in amphibole content (Clemens and Vielzeuf, 1987). As discussed above, no backarc basin rocks have been identified beneath the Western Fiordland Orthogneiss, and hydrous metasedimentary host rocks show little evidence for melting except within the immediate contact aureole of the Western Fiordland Orthogneiss (Allibone et al. 2009b; Daczko et al. 2009). The mantle-like $\delta^{18}O$ (Zrn) values for the Western Fiordland Orthogneiss also preclude significant involvement of high-$\delta^{18}O$ sources like the Deep Cove Gneiss (~10.4‰) or putative underthrusted, hydrothermally altered mafic crust (7–15‰: Gregory and Taylor, 1981; Alt et al., 1986; Staudigel et al., 1995). Numerical simulations of amphibolite partial melting based on repeated injection of basalt into the lower crust also conclude that voluminous magma chambers are not likely to form from basaltic protoliths (Petford and Gallagher, 2001; Dufek and Bergantz, 2005). Direct field and geochemical observations from the lower crust of the Famatinian arc, Argentina, also show little evidence for dehydration melting of amphibole, and instead emphasize the role of fractional crystallization of mantle-derived melts in the diversification of lower and mid-crustal crustal arc rocks (Walker et al. 2015). In Fiordland, the sustained production of Separation Point Suite magmas from 128 to 105 Ma, and especially the production of voluminous mafic to intermediate melts in the Western Fiordland Orthogneiss from 118-114 Ma, also point to a mantle heat source in triggering the terminal Zealandia flare-up.

Partial melting of the subducted crust and hybridization with the mantle

Another possibility is that the distinctive chemistry of the Western Fiordland Orthogneiss reflects interaction of partially melted, subducted eclogite-facies metabasalt and/or metasedimentary rocks with the overlying mantle wedge. Slab-derived melts are thought to occur from partial melting of young crust (~5–10 m.y.: Defant and Drummond, 1990; Peacock et al., 1994), or where torn subducted plates are exposed to mantle flow (Yogodzinski et al. 2001). Thermal models that incorporate temperature-dependent viscosity, and/or non-Newtonian viscosity, predict temperatures in the wedge and the top of the slab higher than the fluidsaturated solidus for both basalt and sediment (e.g., Johnson and Plank, 2000) at normal subduction rates and subducting plate ages (Kelemen et al., 2003; van Keken et al., 2002; Kelemen et al. 2014). Thus, partial melts of eclogite-facies metasedimentary rocks and metabasalts likely make up an important component of arc magmas, particularly in high Mg# andesites (>50), and are abundant features in unusually hot subductions zones where 'tears' and/or young subducting plates yield a larger proportion of eclogitic partial melt relative to the overlying mantle wedge (Kelemen et al., 2003; Moyen et al. 2009; Kelemen et al., 2014).

Magmas generated by partial melting and hybridization of subducted oceanic crust with mantle peridotite have distinctive geochemical features that allow us to compare to Western Fiordland Orthogneiss compositions. Slab melts are typically andesitic to dacitic in composition with high Sr/Y (>100) and Al_2O_3 (>15 wt.%) values, and steeply fractionated REE patterns suggestive of an eclogite residue (e.g., Rapp and Watson, 1995). Primitive andesites (Mg#>60) and high-Mg# andesites (Mg#>50) with high-Sr/Y signatures typically have high Cr (>36 ppm) and Ni (>24), features that are interpreted to reflect hybridization of H_2O-rich, low-temperature melts with the high-temperature mantle wedge (Yogodzinski and Kelemen, 1998; Yogodzinski et al. 2001; Kelemen et al. 2014). Slab melts are also characterized by enrichments in fluid-mobile elements relative to REEs (e.g., high U/Yb, Ce/Yb, Ba/La, and Sr/Nd), signatures that are commonly attributed to an aqueous fluid component with isotopic characteristics of hydrothermally altered MORB (e.g., $^{87}Sr/^{86}Sr$ ~0.7035, $^{143}Nd/^{144}Nd$ ~0.5132, and $^{208}Pb/^{204}Pb$ down to 38) (Rapp et al. 1999). However, melting of sedimentary rocks may also be an important factor in controlling the geochemical budgets of fluid-immobile elements such as Nd, Pb, Hf, and Th (Johnson and Plank, 2000; Plank, 2005), and lavas with potentially large components of slab melt (ca, 10%) are reported from some arcs (e.g., Setouchi, Japan: Shimoda et al. 1998; Hanyu et al., 2002; Tatsumi et al., 2003). Despite evidence in slab melts for potentially significant contributions from high-$\delta^{18}O$ sources such as low-temperature hydrothermally altered MOR crust and sedimentary rocks, olivine from slab melts typically display only weak, <1‰ enrichment in $\delta^{18}O$ values over MORBs (see stippled region in Fig. 5A). Bindeman et al. (2005) proposed that the weak enrichment in slab melts may result from a) partial oxygen isotope equilibration between slab melts and mantle peridotite, and/or b) efficient mixing between partial melts from several different parts of the slab such that higher- and lower-$\delta^{18}O$ components average out to have no net difference from average mantle.

Data from the Western Fiordland Orthogneiss display strong similarities to hybridized slab melts described above. A distinctive feature of the Western Fiordland Orthogneiss is that high Mg# (>50) rocks have high-Sr/Y signatures (Fig. 2F) and high Cr and Ni values that likely reflect reaction of hydrous, eclogite-facies partial melts with peridotite during transport through the mantle wedge. Deep emplacement of some, if not all, of the Western Fiordland Orthogneiss at pressures ≥1.4 GPa (Allibone et al., 2009b) is high enough for igneous garnet to be stable on the liquidus (Green, 1972; Green and Ringwood, 1967, 1968; Chapman et al., 2016); however, primitive Western Fiordland Orthogneiss rocks (e.g., Mg# >50) also have high-Sr/Y signatures, which precludes trace-element enrichment by fractional crystallization alone. Zircon trace-element data support this conclusion as early crystallizing zircons with high Ti values show both heavy rare earth element depletions and high Gd/Yb values relative to other continental arc zircons (Fig. 4D-E). Thus, the high-Sr/Y (WR) signature, high Gd/Yb (Zrn), and distinctive trace-element and isotopic features of high-Mg# rocks from the Western Fiordland Orthogneiss reflect primitive melt compositions, and are not features produced exclusively by fractional crystallization. Moreover, these features support the interpretation that garnet was not only a fractionating phase but also a residual phase in the source region.

Figure 9 shows a series of bulk mixing curves for a variety of sources including adakitic melts (A), mantle wedge melts (W), crustal melts (C) and sediment (S). In Fig. 9A-B, Western Fiordland Orthogneiss samples consistently plot at lower Sr/Y and La/Yb values than expected from pure slab melts ('A' in Fig. 9) consistent with major element chemistry (e.g., Fig. 2F). Western Fiordland Orthogneiss rocks also lie near or between bulk mixing curves for adakite/mantle wedge melts and adakite/sediment melts. In this regard, the Western Fiordland Orthogneiss is similar to lavas from the Aleutians where previous workers have argued for mixing and/or hybridization of slab melts with eclogite-facies metasedimentary rocks and mantle wedge melts (Yogodzinski and Kelemen, 1998; Yogodzinski et al., 2001). A distinguishing feature of our data is that at low $\delta^{18}O$ melt values, Western Fiordland Orthogneiss rocks have higher average $^{87}Sr/^{86}Sr$ values compared to modern slab melts and they plot along the bulk mixing trend between slab melts and metasedimentary rock melts together with lavas from Setouchi, Japan (Fig. 9C). The bulk mixing curve with sediment end member in Fig. 9C yields a sediment input value of ~4-5%, which is similar to values calculated for the modern Kermadec-Hikurangi margin (Gamble et al., 1996), but is less than values observed in Setouchi lavas.

Kelemen et al. (2014) modeled the trace-element composition of melts and fluids in equilibrium with eclogite, and observed that modern, high-Mg# andesites display trends that are consistent with eclogite-facies sediment melt input in both 'typical' arcs and those where slab melts have been observed (Fig. 10). Compared to modeled compositions, Western Fiordland Orthogneiss rocks consistently plot between fluid and melt in equilibrium with eclogite, implying contributions from both sources during melting and melt transport. The Worsley Pluton has the highest Th concentrations of Western Fiordland Orthogneiss rocks and consistently overlaps or plots near modeled eclogite-facies sediment melt compositions. Closer inspection of immobile trace elements in Figure 11 shows that high Mg# rocks from Western Fiordland Orthogneiss are characterized by two distinct groups that define: 1) a low Th/La (<0.1) trend including most Western Fiordland Orthogneiss plutons (Breaksea and Resolution Orthogneisses, Malaspina and some Worsley) and modern MORBs; and 2) a high Th/La (~0.3) trend that characterizes high-Th Worsley rocks, and arc rocks from the Antilles and Aleutians (Plank, 2005). Both subducted Kermadec-Hikurangi sediments (Gamble et al., 1996) and lower crustal sedimentary rocks in the Median Batholith (grey diamonds) are potential sources for the high-Th/La signature; however the lack of observed assimilation or mixing trends in our isotopic data (Fig. 8) argues for subducted metasedimentary melt in the source region rather than crustal contamination at the level of emplacement.

Oxygen isotope signatures in zircons from the Western Fiordland Orthogneiss are also remarkably similar to olivine from modern slab melts (Fig. 5A) with both datasets lying within error of high-temperature mantle. Although not conclusive, $\delta^{18}O$ values in Western Fiordland Orthogneiss zircons are consistent with mixing of slab melts with contributions from eclogite-facies metasediment ± fluids in the source region (Figs. 10C, 11). Coupled with the lack of obvious mixing or AFC trends (Fig. 8), we speculate that efficient homogenization and hybridization with mantle or mantle melts occurred in the source region and/or during transport, and prior to emplacement at the base of the crust.

A petrogenetic flare-up model for the Separation Point Suite

Large abundances of high-Sr/Y rocks are atypical in modern arc environments, except in unusually hot subduction zones characterized by either subduction of young oceanic crust, very slow convergence rates allowing heating and melting of the slab, and/or discontinuous 'tears' that enhance mantle convection in the subducting plate and allow conductive heating from the side, top and bottom (e.g., de Boer et al., 1991, 1988; Defant and Drummond, 1990; Yogodzinski et al., 1994; 1995, 2001; Kelemen et al., 2014). Enhanced mantle melting can also be achieved by 'melt-fluxed melting' in which reaction between hydrous partial melts of subducting metasedimentary rock and/or metabasalt and overlying mantle peridotite leads to increasing melt mass, producing a hybrid 'primary melt' in which more than 90% of the compatible elements (Mg, Fe, Ni, Cr) are derived from the mantle, while most of the alkalis and other incompatible elements come from small degrees of partial melting of subducted crust (e.g., Kelemen, 1986, 1990, 1995; Kelemen et al., 1993, 2003b; Myers et al., 1985; Yogodzinski et al., 1995; Yogodzinski and Kelemen, 1998). Melt-fluxed melting may also be facilitated beneath arcs as melts decompress through the mantle column and dissolve solid mantle minerals, thereby increasing the resulting melt mass (Kelemen, 1986, 1990, 1995; Kelemen et al., 1993, 2014). We speculate that the hybrid 'Cordilleran' arc and high Sr/Y composition of the Western Fiordland Orthogneiss reflects this process.

In addition to melt-fluxed melting, the development of discontinuous 'tears' (e.g., slab-tears or ridge-trench collisions) beneath long-lived continental arcs hold the potential to release large volumes of melts if hot, upwelling asthenosphere is exposed to metasomatized subcontinental lithosphere as postulated to have existed in the Mesozoic beneath the Median Batholith (Panter et al., 2006; McCoy-West et al., 2010; Timm et al., 2010; Scott et al., 2014; Czertowicz et al., 2016; McCoy-West et al., 2015; 2016). Field and geochemical studies in mantle rocks thought to have underlain the Median Batholith show that mantle enrichment occurred during a two-stage, metasomatic processes involving reactive percolation of small amounts of mafic silicate melt and subsequent fluxing of an OH-rich fluid during Mesozoic magmatism beneath the arc (Czertowicz et al., 2016). We postulate that the surge of high-Sr/Y melts in the Median Batholith resulted from partial melting of this enriched mantle source in an usually hot subduction zone where a ‘tear’ or slab window produced from a ridge-trench collision allowed for upwelling asthenosphere to interact with and melt the subducted plate and the hydrous subcontinental lithospheric mantle.

The plate tectonic configuration of the Median Batholith prior to Zealandia break-up in the Cretaceous is difficult to know as much of the Cretaceous oceanic crust has been subducted. Existing palinspastic reconstructions vary greatly; however, all involve subduction of either the Phoenix or Moa plates beneath eastern Gondwana in the Early Cretaceous (e.g., Bradshaw, 1989; Luyendyk, 1995; Sutherland and Hollis, 2001; Mortimer et al., 2005). Bradshaw (1989) proposed that extensional break-up of Zealandia resulted from collision of the Phoenix-Pacific spreading center. Based on radiolarian faunal data, Sutherland and Hollis (2001) suggested that a previously unrecognized plate, the Moa plate, subducted beneath the Median Batholith in the Early Cretaceous and obliquely collided with the eastern Gondwana margin resulting in dextral strike-slip motion. We speculate that collision of either the Phoenix-Pacific or Phoenix-Moa ridges with the eastern Gondwana margin, or the development of a slab tear within the subducting plate, may have been responsible for inducing hot asthenospheric upwelling beneath the downgoing slab, resulting in partial melting of eclogite-facies metasedimentary rocks and metabasalt along the plate edge (Fig. 12). Although speculative, a ridge-trench collision or slab tear model provides a mechanism to explain several of the enigmatic tectonomagmatic features of the Cretaceous Median Batholith including: a) the transition of 'normal', low-Sr/Y arc magmatism to high-Sr/Y magmatism from 136-132 Ma (Fig. 12A-B); b) the rapid generation of large volumes of low-silica, high-Sr/Y melts with mantle-like $\delta^{18}O$ (Zrc) signatures in the Western Fiordland Orthogneiss from 128-114 Ma (Fig. 12B-C); c) the anomalous high-temperature (>900°C) eclogite- to granulite-facies metamorphic event in the lower crust of the Western Fiordland Orthogneiss initiating in the host rocks at ca. 134 Ma and peaking between 116-112 Ma (Fig. 12D) (Hollis et al., 2003; Flowers et al., 2005; Tulloch et al., 2011; Stowell et al., 2014; Schwartz et al., 2016); d) the linear nature of high-Sr/Y plutonism along the axis of the Median Batholith (Tulloch and Kimbrough 2003); and e) the development of transpression and dextral strike-slip motion in Fiordland and along the Gondwana margin after ca. 132 Ma (Sutherland and Hollis, 2001; Daczko et al., 2001; 2002; Marcotte et al., 2005; Klepeis et al., 2004; Allibone and Tulloch, 2008). Foundering of the subducted plate beneath Zealandia and subsequent enhanced mantle upwelling may be related to rapid vertical motions in the crust and collapse of the orogen beginning at 108-106 Ma (Fig. 12D) (Klepeis et al., 2007; 2016). An implication of this model is that subduction-related, asthenospheric-wedge melting ceased to be the primary mechanism for generating melts and transfer of thermal energy to the Median Batholith by ca. 136 Ma (c.f., discussion Tulloch et al 2009b).

Do High-MAR Events Contribute to the Addition of New Continental Crust?

Our geochemical and isotopic results from the lower crust of the Median Batholith reveal that the high-MAR event was primarily driven by mantle melting with important, but volumetrically minor, additions of subducted arc sediment and oceanic crust. As such, we argue that >95% of the exposed Western Fiordland Orthogneiss represents new continental crust added to Gondwana from 128-114 Ma, most of which was emplaced between 118-114 Ma (Schwartz et al. 2017). Given the exposed areal extent of the Western Fiordland Orthogneiss (~2350 km^2), a minimum paleo-thickness of ~30 km derived from structural and metamorphic pressure data (Klepeis et al., 2007; 2016), and an arc segment length of ~80 km during peak flare up (118-114 Ma) and 125 km during the entire duration of the flare up, we calculate a time-averaged lower crustal magma addition rate of ≥38 km^3/Ma/arc-km from 128-114 Ma, and a peak rate of ≥152 km^3/Ma/arc-km from 118-114 Ma during the interval when ~70% of the arc root was emplaced [see Supplementary file for summary of geochronology and flux rate calculations]. When integrated for the entire crustal column, total crustal (0-65 km) magma addition rates are 70 km^3/Ma/arc-km during the surge of magmatism from 128-114 Ma. As the Western Fiordland Orthogneiss shows little if any evidence for crustal interaction, magma addition rates are approximately equal to continental crustal production rates. These rates, however, are minima as they do not include the effects of lateral arc migration during the flare-up interval, a feature that is obscured by the truncation of Western Fiordland by the Alpine Fault. Following Ducea et al. (2015 and 2017), we assume an average arc migration rate of ~4 km/Ma, and calculate a reconstructed time-averaged lower crustal magma addition rate of ≥54 km^3/Ma/arc-km from 128-114 Ma, and a peak rate of ≥210 km^3/Ma/arc-km from 118-114 Ma. Comparable magma addition rates have been determined for thick Andean-type arcs where rates average between 10 and 150 km^3/Ma/arc-km (Ducea et al. 2017). In those cases, half of the total magmatic products are estimated to be mafic additions to the crust in contrast to the Western Fiordland Orthogneiss, which is nearly entirely new mantle addition. Compared to other thickened Andean arcs, peak magmatic production rates in the lower crust of the Median Batholith are equal to and/or exceed the highest reported magma addition rates in other Cordilleran arcs, a feature that we attribute to enhanced mantle melting during propagation of a slab tear/window beneath the arc.

Ducea et al. (2017) noted that modern and ancient island arcs (Jicha and Jagoutz, 2015) and thin continental arcs (e.g., Famatinian arc in the Sierra Valle Fértil-Sierra de Famatina: Ducea et al. 2017) are characterized by much faster magma addition rates that reach 300-400 km^3/Ma/arc-km. As such, they proposed that thin arcs are primary factories for the rapid production of continental crust whereby fast to ultrafast magma addition rates are produced by high arc migration rates across the trench. In the case of the Famatinian arc, ultrafast magmatic buildup included ~50% mafic additions from the mantle, resulting in a continental crust production rate of ~180 km^3/Ma/arc-km (Ducea et al., 2017), which is similar to our calculated crustal production rates in the lower crust of the Median Batholith. In addition, the dominantly 'andesitic' lower crust of the Median Batholith and its trace-element composition approximates bulk lower continental crust (see white diamonds in Fig. 10). Thus, we suggest that high-MAR events involving slab tears/widows may be efficient means of generating continental crust in thickened Cordilleran arcs without requiring further modification (c.f., Kelemen and Behn, 2016). In addition, our isotopic data demonstrate that high-MAR events do not necessarily represent isotopic excursions from dominantly mantle-addition trends (Collins et al., 2011); instead, high-MAR events, particularly those involving lower plate triggering processes, may be important in the rapid generation of new lower arc crust along destructive plate margins.

CONCLUSIONS

Geochemical and Hf- and O-isotopic results from the deep crustal root of the Median Batholith, New Zealand, show that the Cretaceous surge in high-Sr/Y magmatism was primarily sourced from the underlying mantle. We suggest that the high-MAR event was caused by a discontinuous 'tear' or ridge collision event. Development of a slab window and asthenospheric upwelling resulted in widespread partial melting of an isotopically enriched and metasomatized subcontinental lithospheric mantle beneath the Median Batholith, with contributions from subducted, eclogite-facies metasedimentary rocks and metabasalt. We propose that the slab tear/window initiated between ca. 136-128 Ma, at the end of low-Sr/Y arc magmatism and prior to the onset of voluminous high-Sr/Y magmatism. If correct, ridge subduction may be linked to regional transpression and local contraction that commenced at ca. 130 and continued to 105 Ma. Propagation of the putative slab window beneath Zealandia may also explain the apparent gap in magmatism from 136-128 Ma, and the continentward migration of high Sr/Y-magmatism throughout Zealandia. Our isotopic results reveal that the terminal Cretaceous flare-up resulted in the rapid addition of >2350 km^2 of new lower arc crust with time-averaged crustal production rates of ~40-50 km^3/Ma/arc-km from 128-114 Ma, and peak rates of 150-210 km^3/Ma/arc-km from 118-114 Ma when ~70% of the arc root was emplaced. Compared to bulk continental crust, the lower crust of the Median batholith is remarkably similar in trace-element composition, suggesting that high-MAR events involving slab tears or ridge-trench collisions may be an efficient means of generating lower continental crust from hybridization of mantle and subducted slab components, and may not require second stage processes such as relamination (Kelemen and Behn, 2016).

ACKNOWLEDGEMENTS

We acknowledge stimulating discussions with Scott Paterson, Cal Barnes, David Kimbrough, and Robinson Cecil. We thank George Bergantz and Calvin Miller for excellent comments that improved the manuscript. We thank Richard and Mandy Abernethy and the Crew of Fiordland Expeditions for assistance with rock sampling on the Fiordland coast. The New Zealand Department of Conservation, Te Anau office is also thanked for allowing access and sampling in Fiordland. Financial support for this work was provided by NSF grants EAR-1352021 (JJS), EAR-1119039 (HHS & JJS), and EAR-1119248 (KAK). The WiscSIMS laboratory is partly supported by the National Science Foundation EAR-1355590 and by the University of Wisconsin-Madison.

TABLES

Table 1. Summary of zircon U-Pb, O and Lu-Hf isotope data for the Western Fiordland Orthogneiss, Median Batholith, Zealandia Cordillera.

SUPPLEMENTARY FILES

Table 1: Sample locations.

Table 2: Whole-rock geochemistry of the Western Fiordland Orthogneiss.

Table 3: Zircon geochemistry.

Table 4: Oxygen-isotope data.

Table 5: Hf-isotope data.

Table 6: Magma addition rate (MAR) calculations

REFERENCES

Allibone, A. H., Jongens, R., Turnbull, I. M., Milan, L. A., Daczko, N. R., DePaoli, M. C. & Tulloch, A. J. (2009a). Plutonic rocks of Western Fiordland, New Zealand: Field relations, geochemistry, correlation, and nomenclature. *New Zealand Journal of Geology and Geophysics* **52**, 379–415.

Allibone, A. H., Milan, L. A., Daczko, N. R. & Turnbull, I. M. (2009b). Granulite facies thermal aureoles and metastable amphibolite facies assemblages adjacent to the Western Fiordland Orthogneiss in southwest Fiordland, New Zealand. *Journal of Metamorphic Geology* **27**, 349–369.

Allibone, A. H. & Tulloch, A. J. (2004). Geology of the plutonic basement rocks of Stewart Island, New Zealand. *New Zealand Journal of Geology and Geophysics*, 233–256.

Allibone, A. H. & Tulloch, A. J. (2008). Early Cretaceous dextral transpressional deformation within the Median Batholith, Stewart Island, New Zealand. *New Zealand Journal of Geology and Geophysics* **51**, 115–134.

Alt, J. C., Honnorez, J., Laverne, C. & Emmermann, R. (1986). Hydrothermal alteration of a 1 km section through the upper oceanic crust, Deep Sea Drilling Project Hole 504B: Mineralogy, chemistry and evolution of seawater-basalt interactions. *Journal of Geophysical Research* **91**, 10309.

Appleby, S. K., Gillespie, M. R., Graham, C. M., Hinton, R. W., Oliver, G. J. H., Kelly, N. M. & EIMF (2010). Do S-type granites commonly sample infracrustal sources? New results from an integrated O, U-Pb and Hf isotope study of zircon. *Contributions to Mineralogy and Petrology* **160**, 115–132.

Armstrong, R. L. (1988). Mesozoic and early Cenozoic magmatic evolution of the Canadian Cordillera. *Geological Society of America Special Papers* **218**, 55–92.

Barth, A. P. & Wooden, J. L. (2010). Coupled elemental and isotopic analyses of polygenetic zircons from granitic rocks by ion microprobe, with implications for melt evolution and the sources of granitic magmas. *Chemical Geology* **277**, 149–159.

Beck, S. L., Zandt, G., Myers, S. C., Wallace, T. C., Silver, P. G. & Drake, L. (1996). Crustal-thickness variations in the central Andes. *Geology* **24**, 407.

Bindeman, I. N., Eiler, J. M., Yogodzinski, G. M., Tatsumi, Y., Stern, C. R., Grove, T. L., Portnyagin, M., Hoernle, K. & Danyushevsky, L. V. (2005). Oxygen isotope evidence for slab melting in modern and ancient subduction zones. *Earth and Planetary Science Letters* **235**, 480–496.

Blattner, P. (1991). The North Fiordland transcurrent convergence. *New Zealand Journal of Geology and Geophysics* **34**, 533–542.

Blattner, P., Grindley, G. W. & Adams, C. J. (1997). Low-18O terranes tracking Mesozoic polar climates in the South Pacific. *Geochimica et Cosmochimica Acta* **61**, 569–576.

Bolhar, R., Weaver, S. D., Whitehouse, M. J., Palin, J. M., Woodhead, J. D. & Cole, J. W. (2008). Sources and evolution of arc magmas inferred from coupled O and Hf isotope systematics of plutonic zircons from the Cretaceous Separation Point Suite (New Zealand). *Earth and Planetary Science Letters* **268**, 312–324.

Bradshaw, J. Y. (1990). Geology of crystalline rocks of northern Fiordland: Details of the granulite facies Western Fiordland Orthogneiss and associated rock units. *New Zealand Journal of Geology and Geophysics*, 465–484.

Bradshaw, J. Y. (1989). Origin and metamorphic history of an Early Cretaceous polybaric granulite terrain, Fiordland, southwest New Zealand. *Contributions to Mineralogy and Petrology* **103**, 346–360.

Brown, E. (1996). High-pressure metamorphism caused by magma loading in Fiordland, New Zealand. *Journal of Metamorphic Geology* **14**, 441–452.

Cavosie, A. J., Kita, N. T. & Valley, J. W. (2009). Primitive oxygen-isotope ratio recorded in magmatic zircon from the Mid-Atlantic Ridge. *American Mineralogist* **94**, 926–934.

Chapman, A. D., Saleeby, J. B. & Eiler, J. (2013). Slab flattening trigger for isotopic disturbance and magmatic flareup in the southernmost Sierra Nevada batholith, California. *Geology* **41**, 1007–1010.

Chapman, T., Clarke, G. L., Daczko, N. R., Piazolo, S. & Rajkumar, A. (2015). Orthopyroxene–omphacite- and garnet–omphacite-bearing magmatic assemblages, Breaksea Orthogneiss, New Zealand: Oxidation state controlled by high-P oxide fractionation. *Lithos* **216–217**, 1–16.

Chapman, T., Clarke, G. L. & Daczko, N. R. (2016). Crustal Differentiation in a Thickened Arc-Evaluating Depth Dependences. *Journal of Petrology* **57**, 595–620.

Christensen, N. I. & Mooney, W. D. (1995). Seismic velocity structure and composition of the continental crust: A global view. *Journal of Geophysical Research* **100**, 9761-9788.

Clarke, G. L., Klepeis, K. A. & Daczko, N. R. (2002). Cretaceous high-P granulites at Milford Sound, New Zealand: metamorphic history and emplacement in a convergent margin setting. *Journal of Metamorphic Geology* **18**, 359–374.

Clemens, J. D. & Vielzeuf, D. (1987). Constraints on melting and magma production in the crust. *Earth and Planetary Science Letters* **86**, 287–306.

Collins, W. J., Belousova, E. A., Kemp, A. I. S. & Murphy, J. B. (2011). Two contrasting Phanerozoic orogenic systems revealed by hafnium isotope data. *Nature Geoscience* **4**, 333–337.

Cui, Y. & Russell, J. K. (1995). Nd-Sr-Pb isotopic studies of the southern Coast Plutonic Complex, southwestern British Columbia. *Geological Society of America Bulletin*. Geological Society of America **107**, 127-138.

Czertowicz, T. A., Scott, J. M., Waight, T. E., Palin, J. M., Van der Meer, Q. H. A., Le Roux, P., Münker, C. & Piazolo, S. (2016). The Anita Peridotite, New Zealand: Ultra-depletion and Subtle Enrichment in Sub-arc Mantle. *Journal of Petrology*. **57**, 717–750.

Daczko, N. R. & Halpin, J. a. (2009). Evidence for melt migration enhancing recrystallization of metastable assemblages in mafic lower crust, Fiordland, New Zealand. *Journal of Metamorphic Geology* **27**, 167–185.

Daczko, N. R., Klepeis, K. A. & Clarke, G. L. (2001). Evidence of early Cretaceous collisional-style orogenesis in Northern Fiordland, New Zealand and its effects on the evolution of the lower crust. *Journal of Structural Geology* **23**, 693–713.

Daczko, N. R., Klepeis, K. A. & Clarke, G. L. (2002). Thermomechanical evolution of the crust during convergence and deep crustal pluton emplacement in the Western Province of Fiordland, New Zealand. *Tectonics* **21**, 10.1029/2001TC001282.

Daczko, N. R., Stevenson, J. a., Clarke, G. L. & Klepeis, K. a. (2002). Successive hydration and dehydration of high-P mafic granofels involving clinopyroxene-kyanite symplectites, Mt Daniel, Fiordland, New Zealand. *Journal of Metamorphic Geology* **20**, 669–682.

Davy, B., Hoernle, K. & Werner, R. (2008). Hikurangi Plateau: Crustal structure, rifted formation, and Gondwana subduction history. *Geochemistry, Geophysics, Geosystems* **9**,.

de Boer, J.Z., Defant, M.J., Stewart, R.H, and Bellon, H. (1991). Evidence for active subduction below western Panama. *Geology* **19**, 649–652.

de Boer, J.Z., Defant, M.J., Stewart, R.H., Restrepo, J.F., Clark, L.F., and Ramirez, A.H. (1988).

Quaternary calc-alkaline volcanism in western Panama: Regional variation and implication for the plate tectonic framework. *Journal of South American Earth Sciences* **1**, 275–293.

DeCelles, P. G., Ducea, M. N., Kapp, P. & Zandt, G. (2009). Cyclicity in Cordilleran orogenic systems. *Nature Geoscience* **2**, 251–257.

DeCelles, P. G. & Graham, S. A. (2015). Cyclical processes in the North American Cordilleran orogenic system. *Geology* **43**, 499–502.

De Paoli, M. C., Clarke, G. L., Klepeis, K. A., Allibone, A. H. & Turnbull, I. M. (2009). The eclogite-granulite transition: Mafic and intermediate assemblages at Breaksea sound, New Zealand. *Journal of Petrology* **50**, 2307–2343.

Decker, M., 2016, Triggering Mechanisms For A Magmatic Flare-Up Of The Lower Crust In Fiordland, New Zealand, From U-Pb Zircon Geochronology And O-Hf Zircon Geochemistry: California State University Northridge, MS thesis, 122 p.

Dhuime, B., Hawkesworth, C. & Cawood, P. (2011). When Continents Formed. *Science* **331**, 154–155.

Defant, M. J. & Drummond, M. S. (1990). Derivation of some modern arc magmas by melting of young subducted lithosphere. *Nature* **347**, 662–665.

Ducea, M. (2001). The California arc: Thick granitic batholiths, eclogitic residues, lithospheric-scale thrusting, and magmatic flare-ups. *GSA Today* **11**, 4–10.

Ducea, M. N. & Barton, M. D. (2007). Igniting flare-up events in Cordilleran arcs. *Geology* **35**, 1047–1050.

Ducea, M. N., Paterson, S. R. & DeCelles, P. G. (2015a). High-volume magmatic events in subduction systems. *Elements* **11**, 99–104.

Ducea, M. N., Saleeby, J. B. & Bergantz, G. (2015b). The Architecture, Chemistry, and Evolution of Continental Magmatic Arcs. *Annual Review of Earth and Planetary Sciences* **43**, 299–333.

Ducea, M. N., Bergantz, G., Crowley, J. L., Otamendi, J. (2017). Ultrafast magmatic buildup and diversification to produce continental crust during subduction. *Geology* doi: 10.1130/G38726.1.

Eberhart-Phillips, D. & Reyners, M. (2001). A complex, young subduction zone imaged by three-dimensional seismic velocity, Fiordland, New Zealand. *Geophysical Journal International* **146**, 731–746.

Ferry, J.M., & Watson, E.B. (2007). New thermodynamic models and revised calibrations for the Ti-in-zircon and Zr-in-rutile thermometers. *Contributions to Mineralogy and Petrology* **154**, 429–437, doi: 10.1007/s00410-007-0201-0

Flowers, R. M., Bowring, S. A., Tulloch, A. J. & Klepeis, K. A. (2005). Tempo of burial and exhumation within the deep roots of a magmatic arc, Fiordland, New Zealand. *Geology* **33**, 17.

Frost, B. R., Barnes, C. G., Collins, W. J., Arculus, R. J., Ellis, D. J. & Frost, C. D. (2001). A geochemical classification for granitic rocks. *Journal of Petrology* **42**, 2033–2048.

Frost, B. R. & Frost, C. D. (2008). A geochemical classification for feldspathic igneous rocks. *Journal of Petrology* **49**, 1955–1969.

Gamble, J., Woodhead, J., Wright, I. & Smith, I. (1996). Basalt and Sediment Geochemistry and Magma Petrogenesis in a Transect from Oceanic Island Arc to Rifted Continental Margin Arc: the Kermadec—Hikurangi Margin, SW Pacific. *Journal of Petrology* **37**, 1523–1546.

Gibson, G. M. (1992). Medium-high-pressure metamorphic rocks of the Tuhua Orogen, western New Zealand, as lower crustal analogues of the Lachlan Fold Belt, SE Australia. *Tectonophysics* **214**, 145–157.

Gibson, G. M. & Ireland, T. R. (1995). Granulite formation during continental extension in Fiordland, New Zealand. *Nature*, 479–482.

Green, T. H. & Ringwood, A. E. (1967). Crystallization of basalt and andesite under high pressure hydrous conditions. *Earth and Planetary Science Letters* **3**, 481–489.

Green, T. H. & Ringwood, A. E. (1968). Genesis of the calc-alkaline igneous rock suite. *Contributions to Mineralogy and Petrology* **18**, 105–162.

Green, T. H. (1972). Crystallization of calc-alkaline andesite under controlled high-pressure hydrous conditions. *Contributions to Mineralogy and Petrology*. Springer-Verlag **34**, 150–166.

Hanyu, T., Tatsumi, Y. & Nakai, S. (2002). A contribution of slab-melts to the formation of high-Mg andesite magmas; Hf isotopic evidence from SW Japan. *Geophysical Research Letters* **29**, 8-1-8–4.

Haschke, M., Gunther, A., Melnick, D., Echtler, H., Reutter, K. J., Scheuber, E. & Oncken, O. (2006). Central and southern Andean tectonic evolution inferred from arc magmatism. In: Oncken, O., Chong, G., Franz, G., Giese, P., Götze, H.-J., Ramos, H.-J., Strecker, M. R. & Wigger, P. (eds) *The Andes—Active Subduction Orogeny: Frontiers in Earth Sciences*. Berlin: Springer-Verlag, 337–353.

Haschke, M., Siebel, W., Günther, A. & Scheuber, E. (2002). Repeated crustal thickening and recycling during the Andean orogeny in north Chile (21°-26°S). *Journal of Geophysical Research: Solid Earth* **107**, ECV 6-1-ECV 6-18.

Hawkesworth, C. J. & Kemp, A. I. S. (2006). Using hafnium and oxygen isotopes in zircons to unravel the record of crustal evolution. *Chemical Geology* **226**, 144–162.

Hawkesworth, C. J., Dhuime, B., Pietranik, A. B., Cawood, P. A., Kemp, A. I. S. & Storey, C. D. (2010). The generation and evolution of the continental crust. *Journal of the Geological Society* **167**, 229–248.

Hildreth, W. & Moorbath, S. (1988). Crustal contributions to arc magmatism in the Andes of Central Chile. *Contributions to Mineralogy and Petrology* **98**, 455–489.

Hollis, J. A., Clarke, G. L., Klepeis, K. A., Daczko, N. R. & Ireland, T. R. (2003). Geochronology and geochemistry of high-pressure granulites of the Arthur River Complex, Fiordland, New Zealand: Cretaceous magmatism and metamorphism on the palaeo-Pacific Margin. *Journal of Metamorphic Geology* **21**, 299–313.

Hout, C., Stowell, H.H., Schwartz, J.J., Klepeis, K.A. (2012). New ^{206}Pb/^{238}U Zircon Ages Record Magmatism and Metamorphism in the Crustal Root of a Magmatic Arc, Fiordland, New Zealand. *Geological Society of America Abstracts with Programs, 44, No. 7*, 586.

von Huene, R., Ranero, C. R. & Scholl, D. W. (2009). Convergent Margin Structure in High-Quality Geophysical Images and Current Kinematic and Dynamic Models. *Subduction Zone Geodynamics*, 137–157.

Iizuka, T., and Hirata, T. (2005). Improvements of precision and accuracy in in situ Hf isotope microanalysis of zircon using the laser ablation-MC-ICPMS technique. *Chemical Geology* **220,** 121–137.

Johnson, M. C. & Plank, T. (2000). Dehydration and melting experiments constrain the fate of subducted sediments. *Geochemistry, Geophysics, Geosystems* **1**.

Kay, S. M., Godoy, E. & Kurtz, A. (2005). Episodic arc migration, crustal thickening, subduction erosion, and magmatism in the south-central Andes. *Bulletin of the Geological Society of America*. Geological Society of America **117**, 67–88.

van Keken, P. E., B. Kiefer, and S. M. Peacock, (2002). High-resolution models of subduction zones: Implications for mineral dehydration reactions and the transport of water into the deep mantle, Geochem. Geophys. Geosyst., **3**(10), 1056, doi:10.1029/2001GC000256.

Kelemen, P. B. (1990). Reaction between ultramafic rock and fractionating basaltic magma I. phase relations, the origin of calc-alkaline magma series, and the formation of discordant dunite. *Journal of Petrology* **31**, 51–98.

Kelemen, P. B. (1995). Genesis of high Mg# andesites and the continental crust. *Contributions to Mineralogy and Petrology* **120**, 1–19.

Kelemen, P. B. & Ghiorso, M. S. (1986). Assimilation of peridotite in zoned calc-alkaline plutonic complexes: evidence from the Big Jim complex, Washington Cascades. *Contributions to Mineralogy and Petrology* **94**, 12–28.

Kelemen, P. B. & Behn, M. D. (2016). Formation of lower continental crust by relamination of buoyant arc lavas and plutons. *Nature Geoscience* **9**, 197–205.

Kelemen, P. B., Shimizu, N. & Dunn, T. (1993). Relative depletion of niobium in some arc magmas and the continental crust: partitioning of K, Nb, La and Ce during melt/rock reaction in the upper mantle. *Earth and Planetary Science Letters* **120**, 111–134.

Kelemen, P. B., Yogodzinski, G. M. & Scholl, D. W. (2003). Along-Strike Variation in the Aleutian Island Arc: Genesis of High Mg# Andesite and Implications for Continental Crust. *Geophysical Monograph*, 223–276.

Kelemen, P. B., Hanghøj, K. & Greene, A. R. (2014). One View of the Geochemistry of Subduction-Related Magmatic Arcs, with an Emphasis on Primitive Andesite and Lower Crust. *Treatise on Geochemistry*. Elsevier, 749–806.

Kemp, A. I. S., Hawkesworth, C. J., Foster, G. L., Paterson, B. A., Woodhead, J. D., Hergt, J. M., Gray, C. M. & Whitehouse, M. J. (2007). Magmatic and Crustal Differentiation History of Granitic Rocks from Hf-O Isotopes in Zircon. *Science* **315**, 980–983.

Kemp, A. I. S., Hawkesworth, C. J., Collins, W. J., Gray, C. M. & Blevin, P. L. (2009). Isotopic evidence for rapid continental growth in an extensional accretionary orogen: The Tasmanides, eastern Australia. *Earth and Planetary Science Letters* **284**, 455–466.

Kimbrough, D. L., Tulloch, A. J., Coombs, D. S., Landis, C. A., Johnston, M. R. & Mattinson, J. M. (1994). Uranium-lead zircon ages from the Median Tectonic Zone, New Zealand. *New Zealand Journal of Geology and Geophysics* **37**, 393–419.

Kistler, R. W., Wooden, J. L., Premo, W. R. & Morton, D. M. (2014). Pb-Sr-Nd-O isotopic characterization of Mesozoic rocks throughout the northern end of the Peninsular Ranges batholith: Isotopic evidence for the magmatic evolution of oceanic arc–continental margin accretion during the Late Cretaceous of southern California. *Peninsular Ranges Batholith, Baja California and Southern California.* In: Morton, D. M. & Miller, F. (eds) *Geological Society of America Memoirs* **211**, 263–316.

Klepeis, K. A. & Clarke, G. L. (2004). The evolution of an exposed mid-lower crustal attachment zone in Fiordland, New Zealand. *Geological Society, London, Special Publications* **227**, 197–229.

Klepeis, K. A., Clarke, G. L., Gehrels, G. & Vervoort, J. (2004). Processes controlling vertical coupling and decoupling between the upper and lower crust of orogens: Results from Fiordland, New Zealand. *Journal of Structural Geology* **26**, 765–791.

Klepeis, K. A., King, D., De Paoli, M., Clarke, G. L. & Gehrels, G. (2007). Interaction of strong lower and weak middle crust during lithospheric extension in western New Zealand. *Tectonics* **26,** doi: 10.1029/2006TC002003.

Klepeis, K. A., Schwartz, J., Stowell, H. & Tulloch, A. (2016). Gneiss domes, vertical and horizontal mass transfer, and the initiation of extension in the hot lower-crustal root of a continental arc, Fiordland, New Zealand. *Lithosphere* **8**, 116–140.

Kolodny, Y. & Epstein, S. (1976). Stable isotope geochemistry of deep sea cherts. *Geochimica et Cosmochimica Acta* **40**, 1195–1209.

Lackey, J. S., Valley, J. W. & Saleeby, J. B. (2005). Supracrustal input to magmas in the deep crust of Sierra Nevada batholith: Evidence from high-δ^{18}O zircon. *Earth and Planetary Science Letters* **235**, 315–330.

Lackey, J.S., Valley, J.W., and Hinke, H.J. (2006). Deciphering the source and contamination history of peraluminous magmas using δ^{18}O of accessory minerals: Examples from garnet-bearing plutons of the Sierra Nevada batholith. *Contributions to Mineralogy and Petrology*, **151**, 20–44.

Lackey, J. S., Valley, J. W., Chen, J. H. & Stockli, D. F. (2008). Dynamic magma systems, crustal recycling, and alteration in the Central Sierra Nevada batholith: The oxygen isotope record. *Journal of Petrology* **49**, 1397–1426.

Lackey, J. S., Cecil, M. R., Windham, C. J., Frazer, R. E., Bindeman, I. N. & Gehrels, G. E. (2012). The Fine Gold Intrusive Suite: The roles of basement terranes and magma source development in the Early Cretaceous Sierra Nevada batholith. *Geosphere* **8**, 292–313.

Lee, C. T. A., Cheng, X. & Horodyskyj, U. (2006). The development and refinement of continental arcs by primary basaltic magmatism, garnet pyroxenite accumulation, basaltic recharge and delamination: Insights from the Sierra Nevada, California. *Contributions to Mineralogy and Petrology* **151**, 222–242.

Luyendyk, B. P. (1995). Hypothesis for Cretaceous rifting of east Gondwana caused by subducted slab capture. *Geology* **23**, 373–376.

Marcotte, S. B., Klepeis, K. A., Clarke, G. L., Gehrels, G. & Hollis, J. A. (2005). Intra-arc transpression in the lower crust and its relationship to magmatism in a Mesozoic magmatic arc. *Tectonophysics* **407**, 135–163.

Mattinson, J. M., Kimbrough, D. L. & Bradshaw, J. Y. (1986). Western Fiordland orthogneiss: Early Cretaceous arc magmatism and granulite facies metamorphism, New Zealand. *Contributions to Mineralogy and Petrology* **92**, 383–392.

Martin, H., Smithies, R. H., Rapp, R., Moyen, J. F. & Champion, D. (2005). An overview of adakite, tonalite-trondhjemite-granodiorite (TTG), and sanukitoid: Relationships and some implications for crustal evolution. *Lithos*, 1–24.

McCoy-West, A., Mortimer, N. & Ireland, T. R. (2014). U-Pb geochronology of Permian plutonic rocks, Longwood Range, New Zealand: Implications for Median Batholith-Brook Street Terrane relations. *New Zealand Journal of Geology and Geophysics* **57**, 65–85.

McCoy-West, A. J., Baker, J. a., Faure, K. & Wysoczanski, R. (2010). Petrogenesis and origins of mid-cretaceous continental intraplate volcanism in Marlborough, New Zealand:

Implications for the long-lived HIMU magmatic mega-province of the SW Pacific. *Journal of Petrology* **51**, 2003–2045.

McCoy-West, A. J., Bennett, V. C., O'Neill, H. S. C., Hermann, J. & Puchtel, I. S. (2015). The Interplay between Melting, Refertilization and Carbonatite Metasomatism in Off-Cratonic Lithospheric Mantle under Zealandia: an Integrated Major, Trace and Platinum Group Element Study. *Journal of Petrology* **56**, 563–604.

McCoy-West, A.J., Bennett, V.C., and Amelin, Y. (2016). Rapid Cenozoic ingrowth of isotopic signatures simulating "HIMU" in ancient lithospheric mantle: Distinguishing source from process. *Geochimica et Cosmochimica Acta* **187**, p. 79–101.

McCulloch, M. T., Bradshaw, J. Y. & Taylor, S. R. (1987). Sm-Nd and Rb-Sr isotopic and geochemical systematics in Phanerozoic granulites from Fiordland, southwest New Zealand. *Contributions to Mineralogy and Petrology* **97**, 183–195.

McDonough, W. F. & Sun, S. (1995). The composition of the Earth. *Chemical Geology* **120**, 223–253.

McLennan S. M. and Taylor S. R. (1985) *The Continental Crust: Its Composition and Evolution: An Examination of the Geochemical Record Preserved in Sedimentary Rocks*. Blackwell Scientific, Oxford

Milan, L. A., Daczko, N. R., Clarke, G. L. & Allibone, A. H. (2016). Complexity of In-situ zircon U–Pb–Hf isotope systematics during arc magma genesis at the roots of a Cretaceous arc, Fiordland, New Zealand. *Lithos* **264**, 296–314.

Mortimer, N. *et al.* (2014). High-level stratigraphic scheme for New Zealand rocks. *New Zealand Journal of Geology and Geophysics* **57**, 402–419.

Mortimer, N., Tulloch, a. J., Spark, R. N., Walker, N. W., Ladley, E., Allibone, A. & Kimbrough, D. L. (1999). Overview of the Median Batholith, New Zealand: A new interpretation of the geology of the Median Tectonic Zone and adjacent rocks. *Journal of African Earth Sciences* **29**, 257–268.

Mortimer, N. et al. (2017). Zealandia: Earth's Hidden Continent. GSA Today 27–35.

Moyen, J. F. (2009). High Sr/Y and La/Yb ratios: The meaning of the "adakitic signature." *Lithos* **112**, 556–574.

Muir, R. J., Weaver, S. D., Bradshaw, J. D., Eby, G. N. & Evans, J. A. (1995). The Cretaceous Separation Point batholith, New Zealand: granitoid magmas formed by melting of mafic lithosphere. *Journal of the Geological Society* **152**, 689–701.

Muir, R. J., Ireland, T. R., Weaver, S. D., Bradshaw, J. D., Evans, J. a., Eby, G. N. & Shelley, D. (1998). Geochronology and geochemistry of a Mesozoic magmatic arc system, Fiordland, New Zealand. *Journal of the Geological Society* **155**, 1037–1053.

Oliver, G. J. H. (1977). Feldspathic hornblende and garnet granulites and associated anorthosite pegmatites from Doubtful Sound, Fiordland, New Zealand. *Contributions to Mineralogy and Petrology* **65**, 111–121.

Oliver, G. J. H. (1980). Geology of the granulite and amphibolite facies gneisses of Doubtful Sound, Fiordland, New Zealand. *New Zealand Journal of Geology and Geophysics* **23**, 27–41.

Oliver, G. J. H. (1976). High grade metamorphic rocks of Doubtful Sound, Fiordland, New Zealand—a study of the lower crust. PhD thesis: University of Otago.

De Paoli, M. C., Clarke, G. L., Klepeis, K. A., Allibone, A. H. & Turnbull, I. M. (2009). The Eclogite-Granulite Transition: Mafic and Intermediate Assemblages at Breaksea Sound, New Zealand. *Journal of Petrology* **50**, 2307–2343.

Page, F. Z., Ushikubo, T., Kita, N. T., Riciputi, L. R. & Valley, J. W. (2007). High-precision oxygen isotope analysis of picogram samples reveals 2 μm gradients and slow diffusion in zircon. *American Mineralogist* **92**, 1772–1775.

Panter, K. S., Blusztajn, J., Hart, S. R., Kyle, P. R., Esser, R. & McIntosh, W. C. (2006). The origin of HIMU in the SW Pacific: Evidence from intraplate volcanism in Southern New Zealand and Subantarctic Islands. *Journal of Petrology* **47**, 1673–1704.

Patchett, P. J. & Tatsumoto, M. (1980). Hafnium isotope variations in oceanic basalts. *Geophysical Research Letters* **7**, 1077–1080.

Patchett, P. J. & Tatsumoto, M. (1981). A routine high-precision method for Lu-Hf isotope geochemistry and chronology. *Contributions to Mineralogy and Petrology* **75**, 263–267.

Paterson, S. R., Okaya, D., Memeti, V., Economos, R. & Miller, R. B. (2011). Magma addition and flux calculations of incrementally constructed magma chambers in continental margin arcs: Combined field, geochronologic, and thermal modeling studies. *Geosphere* **7**, 1439–1468.

Paterson, S. R. & Ducea, M. N. (2015). Arc magmatic tempos: Gathering the evidence. *Elements* **11**, 91–98.

Paton, C., Hellstrom, J., Paul, B., Woodhead, J. & Hergt, J. (2011). Iolite: Freeware for the visualisation and processing of mass spectrometric data. *Journal of Analytical Atomic Spectrometry* **26**, 2508–2518.

Peacock, S. M., Rushmer, T. & Thompson, A. B. (1994). Partial melting of subducting oceanic crust. *Earth and Planetary Science Letters* **121**, 227–244.

Petford, N. & Gallagher, K. (2001). Partial melting of mafic (amphibolitic) lower crust by periodic influx of basaltic magma. *Earth and Planetary Science Letters* **193**, 483–499.

Plank, T. (2005). Constraints from Thorium/Lanthanum on Sediment Recycling at Subduction Zones and the Evolution of the Continents. *Journal of Petrology* **46**, 921–944.

Ramezani, J. Tulloch, A.J. (2009). TIMS U-Pb geochronology of southern and eastern Fiordland: http://data.gns.cri.nz/paperdata/index.jsp.

Ramos, V. A. (2009). Anatomy and global context of the Andes: Main geologic features and the Andean orogenic cycle. *Backbone of the Americas: Shallow Subduction, Plateau Uplift, and Ridge and Terrane Collision: Geological Society of America Memoirs*. Geological Society of America **1204**, 31–65.

Ramos, V. A., Litvak, V. D., Folguera, A. & Spagnuolo, M. (2014). An Andean tectonic cycle: From crustal thickening to extension in a thin crust (34°–37°SL). *Geoscience Frontiers* **5**, 351–367.

Rapp, R. P. & Watson, E. B. (1995). Dehydration melting of metabasalt at 8-32 kbar: Implications for continental growth and crust-mantle recycling. *Journal of Petrology* **36**, 891–931.

Rapp, R. P., Shimizu, N., Norman, M. D. & Applegate, G. S. (1999). Reaction between slab-derived melts and peridotite in the mantle wedge: Experimental constraints at 3.8 GPa. *Chemical Geology* **160**, 335–356.

Rudnick, R. L. & Fountain, D. M. (1995). Nature and Composition of the Continental-Crust - a Lower Crustal Perspective. *Reviews of Geophysics* **33**, 267–309.

Saleeby, J. (2003). Segmentation of the Laramide Slab—evidence from the southern Sierra Nevada region. *Geological Society of America Bulletin* **115**, 655–668.

Scholl, D. W. & von Huene, R. (2007). Crustal recycling at modern subduction zones applied to the past—Issues of growth and preservation of continental basement crust, mantle geochemistry, and supercontinent reconstruction. *Geological Society of America Memoirs*, 9–32.

Schwartz, J. J., Stowell, H. H., Klepeis, K. A., Tulloch, A. J., Kylander-Clark, A. R. C., Hacker, B. R. & Coble, M. A. (2016). Thermochronology of extensional orogenic collapse in the deep crust of Zealandia. *Geosphere* **12**, 647–677.

Schwartz, J.J., Klepeis, K.A., Sadorski, J.F., Stowell, H.H., Tulloch, A.J., and Coble, M. (2017). The Tempo of Continental Arc Construction in the Mesozoic Median Batholith, Fiordland, New Zealand. *Lithosphere* (doi:10.1130/L610.1)

Scott, J. M. & Palin, J. M. (2008). LA-ICP-MS U-Pb zircon ages from Mesozoic plutonic rocks in eastern Fiordland, New Zealand. *New Zealand Journal of Geology and Geophysics* **51**, 105–113.

Scott, J. M., Cooper, A. F., Palin, J. M., Tulloch, A. J., Kula, J., Jongens, R., Spell, T. L. & Pearson, N. J. (2009). Tracking the influence of a continental margin on growth of a magmatic arc, Fiordland, New Zealand, using thermobarometry, thermochronology, and zircon U-Pb and Hf isotopes. *Tectonics* **28**.

Scott, J. M., Cooper, A. F., Tulloch, A. J. & Spell, T. L. (2011). Crustal thickening of the Early Cretaceous paleo-Pacific Gondwana margin. *Gondwana Research* **20**, 380–394.

Scott, J. M. (2013). A review of the location and significance of the boundary between the Western Province and Eastern Province, New Zealand. *New Zealand Journal of Geology and Geophysics* **56**, 276–293.

Scott, J. M., Waight, T. E., van der Meer, Q. H. A., Palin, J. M., Cooper, A. F. & Münker, C. (2014). Metasomatized ancient lithospheric mantle beneath the young Zealandia microcontinent and its role in HIMU-like intraplate magmatism. *Geochemistry, Geophysics, Geosystems* **15**, 3477–3501.

Shimoda, G., Tatsumi, Y., Nohda, S., Ishizaka, K. & Jahn, B. M. (1998). Setouchi high-Mg andesites revisited: Geochemical evidence for melting of subducting sediments. *Earth and Planetary Science Letters* **160**, 479–492.

Shea, E. K., Miller, J. S., Miller, R. B., Bowring, S. A. & Sullivan, K. M. (2016). Growth and maturation of a mid- to shallow-crustal intrusive complex, North Cascades, Washington. *Geosphere* **12**, 1489–1516.

de Silva, S. L., Riggs, N. R., Barth, A. P., Silva, S. L. De, Riggs, N. R. & Barth, A. P. (2015). Quickening the Pulse: Arc Magmatism. *Elements* **11**, 113–118.

Silver, L. T., Taylor, H. P., & Chappell, B. W. (1979). Some petrological, geochemical and geochronological observations of the Peninsular Ranges batholith near the international border of the USA and Mexico. In *Mesozoic Crystalline Rocks: Geological Society of America, Annual Meeting, Guidebook* (pp. 83-110).

Spicuzza, M.J., Valley, J.W., Kohn, M.J, Girard, J.P., Fouillac, A.M. (1998a). The rapid heating, defocused beam technique: a CO_2-laser based method for highly precise and accurate determination of $\delta^{18}O$ values of quartz. *Chemical Geology* **144,** 195–203.

Spicuzza, M.J., Valley, J.W., McConnell, V.S. (1998b). Oxygen isotope analysis of whole rock via laser fluorination: An air-lock approach. *Geological Society of America Abstracts* **30**, 80.

Staudigel, H., Davies, G. R., Hart, S. R., Marchant, K. M. & Smith, B. M. (1995). Large scale isotopic Sr, Nd and O isotopic anatomy of altered oceanic crust: DSDP/ODP sites417/418. *Earth and Planetary Science Letters* **130**, 169–185.

Stowell, H., Parker, K. O., Gatewood, M., Tulloch, a. & Koenig, a. (2014). Temporal links between pluton emplacement, garnet granulite metamorphism, partial melting and extensional collapse in the lower crust of a Cretaceous magmatic arc, Fiordland, New Zealand. *Journal of Metamorphic Geology* **32**, 151–175.

Sutherland, R. & Hollis, C. (2001). Cretaceous demise of the Moa plate and strike-slip motion at the Gondwana margin. *Geology* **29**, 279–282.

Tatsumi, Y., Shukuno, H., Sato, K., Shibata, T. & Yoshikawa, M. (2003). The Petrology and Geochemistry of High-Magnesium Andesites at the Western Tip of the Setouchi Volcanic Belt, SW Japan. *Journal of Petrology* **44**, 1561–1578.

Tatsumi, Y. & Stern, R. (2006). Manufacturing Continental Crust in the Subduction Factory. *Oceanography* **19**, 104–112.

Taylor, H. P., & Silver, L. T. (1978). Oxygen isotope relationships in plutonic igneous rocks of the Peninsular Ranges batholith, southern and Baja California. *US Geological Survey Open-File Report*, 78-701.

Taylor, S. R. & McLennan, S. M. (1995). The geochemical evolution of the continental crust. *Reviews of Geophysics* **33**, 241.

Thirlwall, M. F. & Anczkiewicz, R. (2004). Multidynamic isotope ratio analysis using MC-ICP-MS and the causes of secular drift in Hf, Nd and Pb isotope ratios. *International Journal of Mass Spectrometry* **235**, 59–81.

Timm, C., Hoernle, K., Werner, R., Hauff, F., den Bogaard, P. Van, White, J., Mortimer, N. & Garbe-Schönberg, D. (2010). Temporal and geochemical evolution of the Cenozoic intraplate volcanism of Zealandia. *Earth-Science Reviews*, 38–64.

Tollstrup, D. L. & Gill, J. B. (2005). Hafnium systematics of the Mariana arc: Evidence for sediment melt and residual phases. *Geology*. **33**, 737–740.

Tulloch, A. J. & Challis, G. A. (2000). Emplacement depths of Paleozoic-Mesozoic plutons from western New Zealand estimated by hornblende-Al geobarometry. *New Zealand Journal of Geology and Geophysics* **43**, 555–567.

Tulloch, A. J. & Kimbrough, D. L. (2003). Paired plutonic belts in convergent margins and the development of high Sr/Y magmatism: Peninsular Ranges batholith of Baja-California and Median batholith of New Zealand. *Geological Society of America, Special Paper* **374**, 275–295.

Tulloch, A. J., Ramezani, J., Kimbrough, D. L., Faure, K. & Allibone, A. H. (2009a). U-Pb geochronology of mid-Paleozoic plutonism in western New Zealand: Implications for S-type granite generation and growth of the east Gondwana margin. *Geological Society of America Bulletin* **121**, 1236–1261.

Tulloch, A. J., Ramezani, J., Mortimer, N., Mortensen, J., van den Bogaard, P. & Maas, R. (2009b). Cretaceous felsic volcanism in New Zealand and Lord Howe Rise (Zealandia) as a precursor to final Gondwana break-up. *Geological Society, London, Special Publications* **321**, 89–118.

Tulloch, A. J., Ireland, T. R., Kimbrough, D. L., Griffin, W. L. & Ramezani, J. (2011). Autochthonous inheritance of zircon through Cretaceous partial melting of Carboniferous plutons: The Arthur River Complex, Fiordland, New Zealand. *Contributions to Mineralogy and Petrology* **161**, 401–421.

Valley, J. W. (2003). Oxygen Isotopes in Zircon. *Reviews in Mineralogy and Geochemistry* **53**, 343–385.

Valley, J. W., Bindeman, I. N. & Peck, W. H. (2003). Empirical calibration of oxygen isotope fractionation in zircon. *Geochimica et Cosmochimica Acta* **67**, 3257–3266.

Valley, J. W., Kitchen, N., Kohn, M. J., Niendorf, C. R. & Spicuzza, M. J. (1995). UWG-2, a garnet standard for oxygen isotope ratios: Strategies for high precision and accuracy with laser heating. *Geochimica et Cosmochimica Acta* **59**, 5223–5231.

Valley, J. W., Lackey, J.S., Cavosie, A.J., Clechenko, C.C., Spicuzza, M.J., Basei, M.A.S., Bindeman, I.N., Ferreira, V.P., Sial, A.N., King, E.M., Peck, W.H., Sinha, A.K., Wei, C.S. (2005). 4.4 billion years of crustal maturation: oxygen isotope ratios of magmatic zircon. *Contributions to Mineralogy and Petrology* **150**, 561–580.

Valley, J. W. & Kita, N. T. (2009). In situ oxygen isotope geochemistry by ion microprobe. *Secondary Ion Mass Spectrometry in the Earth Sciences. Mineralogical Association of Canada, Short Courses* **41**, 19–63.

Vervoort, J. D., Patchett, P. J., Söderlund, U. & Baker, M. (2004). Isotopic composition of Yb and the determination of Lu concentrations and Lu/Hf ratios by isotope dilution using MC-ICPMS. *Geochemistry, Geophysics, Geosystems* **5**, 10.1029/2004GC000721.

Vervoort, J. D. & Blichert-Toft, J. (1999). Evolution of the depleted mantle: Hf isotope evidence from juvenile rocks through time. *Geochimica et Cosmochimica Acta* **63**, 533–556.

Voice, P. J., Kowalewski, M. & Eriksson, K. A. (2011). Quantifying the Timing and Rate of Crustal Evolution: Global Compilation of Radiometrically Dated Detrital Zircon Grains. *The Journal of Geology* **119**, 109–126.

Walker, B. A. Jr., Bergantz, G. W., Otamendi, J. E., Ducea, M. N., & Cristofolini, E. A. (2015). *Journal of Petrology* **56** 1863–1896.

Wang X-L., Coble M.A., Valley J.W., Shu X-J., Kitajima K., Spicuzza M.J., Sun T., (2014). Influence of radiation damage on late Jurassic zircon from southern China: Evidence from in situ measurement of oxygen isotopes, laser Raman, U-Pb ages, and trace elements. *Chemical Geology* **389**, 122-136.

Weaver B. L. & Tarney J. (1984) Empirical approach to estimating the composition of the continental crust. *Nature* **310**, 575–577.

Yogodzinski, G. M. & Kelemen, P. B. (1998). Slab melting in the Aleutians: implications of an ion probe study of clinopyroxene in primitive adakite and basalt. *Earth and Planetary Science Letters* **158**, 53–65.

Yogodzinski, G. M., Volynets, O. N., Koloskov, A. V., Seliverstov, N. I. & Matvenkov, V. V. (1994). Magnesian andesites and the subduction component in a strongly calc-alkaline series at Piip volcano, far western Aleutians. *Journal of Petrology* **35**, 163–204.

Yogodzinski, G. M., Kay, R. W., Volynets, O. N., Koloskov, A. V. & Kay, S. M. (1995). Magnesian andesite in the western Aleutian Komandorsky region: implications for slab melting and processes in the mantle wedge. *Geological Society of America Bulletin*, 505–519.

Yogodzinski, G. M., Lees, J. M., Churikova, T. G., Dorendorf, F., Wöerner, G. & Volynets, O. N. (2001). Geochemical evidence for the melting of subducting oceanic lithosphere at plate edges. *Nature* **409**, 500–504.

FIGURES

Figure 1. A simplified geologic map of the study area in Fiordland (adapted from Allibone et al., 2009a). Samples for zircon O- and Hf isotope analyses are shown with white stars. Inboard Median Batholith consists of Western Fiordland Orthogneiss, which was emplaced during an arc flare-up event from 124-114 Ma.

Figure 2. Bivariate plots of whole-rock data showing geochemical features of the Western Fiordland Orthogneiss (this study and Wiesenfeld and Schwartz, unpublished data). a) Samples range from ~47-60 wt.% SiO_2 and are classified as basalt/trachy-basalt to trachy-andesite. Western Fiordland Orthogneiss samples are largely magnesian (b), calc-alkalic to alkali-calcic (c) and metaluminous (d). e) Molar Mg#s range from 42-60 consistent with fractionation of high-density assemblages including garnet + clinopyroxene from a primitive basalt or primitive andesite. f) Western Fiordland Orthogneiss samples have high-Sr/Y values (>40) indicating the presence of garnet and/or amphibole as residual or fractionating phase. The high Sr/Y character is present and highest in the most primitive samples (Mg# >50) indicating that the high-Sr/Y signature is a feature of the source and not related to crystal fractionation processes. Fields in b-c from Frost et al. (2001, 2008). Fields in e-f compiled from Rapp et al. (1999) and Moyen et al. (2009). BADR = basalt-andesite-dacite-rhyolite arc trend.

Figure 3. Cathodoluminescence images of representative zircons from the Western Fiordland Orthogneiss. Locations of ion microprobe and laser ablation spots shown, U-Pb in white, oxygen in teal, and Hf in yellow along with data from each spot. Scale bars are 100 μm.

Figure 4. Bivariate plots of Western Fiordland Orthogneiss zircon trace-element data compared to the global compilation of zircons from various tectonic environments from Grimes et al. (2015) and references therein. a) U/Yb vs. Hf (ppm) showing enrichment in U/Yb for Western Fiordland Orthogneiss zircons relative to continental arc zircons, suggesting either strong crustal input or an enriched mantle source. b) U/Yb vs. Gd/Yb illustrating the strong garnet signature relative to continental zircons, especially the Worsley and Malaspina Plutons and Breaksea Orthogneiss. Negative trends are consistent with fractional crystallization during cooling. c) Gd/Yb vs. Ce/Yb. Western Fiordland Orthogneiss zircon display enrichment in both Ce/Yb and Gd/Yb, indicating relatively oxidizing magmas relative to MOR, intraplate and other continental zircons. Only zircons from kimberlites have higher average Gd/Yb values. d) Ti vs. Yb showing relatively high Ti concentrations (and high crystallization temperatures) at low average Yb concentrations relative to other continental arc zircons. Weak trends towards decreasing Yb are consistent with either garnet and/or late-stage amphibole crystallization. e) Ti vs. Gd/Yb. Western Fiordland Orthogneiss zircons plot at the high-temperature (Ti) end of the continental arc spectrum, with high Gd/Yb values consistent with a garnet signature. Weak cooling trends are present with either garnet or apatite fractionation.

Figure 5. a) Histogram showing $\delta^{18}O$ (Zrn) values for the Western Fiordland Orthogneiss. Grey bar reflects the $\delta^{18}O$ composition of high-temperature mantle (Valley et al., 2005). The weighted-average $\delta^{18}O$ value for all Western Fiordland Orthogneiss zircons is 5.76 ±

0.04‰ (2σ). Dashed area shows modern ‘adakites’ and high-Mg andesites from global compilation of Bindeman et al. (2005). b) Histogram showing initial εHf (Zrn) for the Western Fiordland Orthogneiss. The weighted-average value for all Western Fiordland Orthogneiss zircons is +4.2 ± 0.2 (2σ). Grey bar reflects the composition of depleted mantle at ca. 120 Ma (Vervoort and Blitchert-Toft, 1999).

Figure 6. Bivariate plots of O-isotope and initial εHf values versus zircon Pb/U age and latitude. a) Bivariate plot of $^{206}Pb/^{238}U$ zircon age vs. $\delta^{18}O$ (Zrn). b) Bivariate plot of $\delta^{18}O$ (Zrn) vs. latitude. c) Bivariate plot of $^{206}Pb/^{238}U$ vs. initial εHf (Zrn). D) Bivariate plot of initial εHf (Zrn) vs. latitude. Grey field in a) and c) reflects the $\delta^{18}O$ composition of zircon in equilibrium with high-temperature mantle (Valley et al., 2005). All Western Fiordland Orthogneiss O-isotope data lie within SIMS analytical error of the mantle field. Grey circles are Western Fiordland Orthogneiss zircons reported in Milan et al. (2016) filtered for $^{206}Pb/^{238}U$ zircon dates between 110 to 130 Ma--the age range of the Western Fiordland Orthogneiss defined by high-precision zircon dates (see Schwartz et al. 2017 and references therein).

Figure 7. Comparison of calculated and measured $\delta^{18}O$ (WR). Calculated values were determined from zircon O-isotopes and SiO_2 concentrations following the equation in Lackey et al. (2008). The grey field bounding the equilibrium line is 3SD of analytical uncertainty wide. Samples that lie off that line are interpreted to have interacted with low-$\delta^{18}O$ (marine or meteoric) water.

Figure 8. Results of bulk mixing (a-b) and assimilation-fractional crystallization (c-d) models for zircon $\delta^{18}O$ and initial εHf (Zrn) data (colored curves). Black, horizontal lines at the bottom of A-D show results of oxygen isotope bulk mass balance mixing models. All

models use a variety of mantle-derived melts. Models in a) and c) use average Deep Cove Gneiss, whereas models in b) and d) use average pelagic sediments (after Vervoort et al. 1999). Ticks and percentages indicate relative proportions of assimilant. In general, models involving Cretaceous depleted mantle (εHf=+15) and average arc (εHf=+13) fail to describe the variation in Western Fiordland Orthogneiss data. Best-fit models involve 'enriched' mantle sources (mixing curves with eHf =+7 to +3 as end member compositions). Results permit bulk mixing and/or assimilation of up to 15% Deep Cove Gneiss and up to 10% pelagic sediment; however, the lack of apparent assimilation or mixing trends suggests that the isotopic composition of Western Fiordland Orthogneiss magmas was acquired in source region rather than by crustal assimilation at the level of emplacement. Mantle arrays after Patchett & Tatsumoto (1980) and Valley et al. (2005).

Figure 9. Bivariate plots of δ^{18}O melt calculated from zircon values versus whole-rock trace-element ratios and initial ^{87}Sr/^{86}Sr. a) Sr/Y vs. δ^{18}O melt. b) La/Yb vs. δ^{18}O melt. c) initial ^{87}Sr/^{86}Sr vs. δ^{18}O melt (Wiesenfeld, unpublished data). Thick black bars in each graph show the accepted range of δ^{18}O for mantle-derived basaltic melts. Curves represent bulk mixing of end member compositions after Bindeman et al. (2005): A—adakitic (slab) melts, W—mantle wedge melts, C—crustal melts, S—sediment melts ± fluids. Fields for global slab melts after Bindeman et al. (2005) and references therein. No La/Yb data are reported for Setouchi, Japan (Fig. 9b). Trace-element data from the Western Fiordland Orthogneiss overlap field defined by Aleutians and lie between bulk mixing curves for adakite-mantle wedge melts and adakite-sediment melts. Radiogenic isotope data plot along the bulk mixing curve for adakite-sediment melt, and indicate ~4-

5% sediment input. Low, Sr/Y lavas from Setouchi, Japan lie along the same bulk mixing curve with higher amounts of sediment input.

Figure 10. Bivariate trace-element plots for Western Fiordland Orthogneiss samples filtered to show only high Mg# basalts and andesites (Mg# >50). In general, Western Fiordland Orthogneiss samples show strong enrichment in Th, Ba, La, Pb, Ce, Sr and Nd, and largely plot within fields defined by other high-Mg# andesites (fields after Kelemen et al., 2014). Large symbols show estimated compositions of fluid (rectangles) and melt (circles) in equilibrium with eclogite for Marianas (blue) and Aleutians (peach) at 2 wt.% fluid or melt extracted (Kelemen et al., 2014). Data from the Western Fiordland Orthogneiss plot between eclogite fluid and melt compositions, suggesting contributions from both sources during melting and melt transport. Relative to bulk continental crust (filled white diamonds), Western Fiordland Orthogneiss is more enriched in Ba, Sr, and somewhat lower in Th. Estimated bulk continental crust values from Christensen and Mooney (1995), McLennan and Taylor (1985), Rudnick and Fountain (1995), and Weaver and Tarney (1984), including Archean estimate of Taylor and McLennan (1995).

Figure 11. Bivariate plots of a) Th/Nb versus La/Nb and b) Th/La versus Sm/La for high-Mg# basalts and andesites (Mg# >50). Fields show modern arc lavas and mid-ocean ridge basalts (MORBs), and sediments from the Kermadec-Hikurangi arc. a) Western Fiordland Orthogneiss data show two trends: 1) a low Th/La (<0.1) source that characterizes the Breaksea and Resolution Orthogneisses, the Malaspina Pluton, some of the Worsley Pluton, and MORBs; and 2) a high Th/La (~0.3) source that characterizes a subgroup of the high-Th, Worsley samples. The high Th/La source is consistent with subducted, Kermadec-Hikurangi sediments (Gamble et al., 1996); b) Western Fiordland

Orthogneiss rocks are characterized by low Sm/La, a feature that also defines OIB, E-MORB and mantle xenoliths from greater Zealandia (Sun and McDonough, 1989; McCoy-West et al., 2015). Western Fiordland Orthogneiss rocks trend from low Th/La to higher values consistent with interaction with high-Th sediment. The black line shows bulk mixing trend between a high-Th sedimentary component and a low-Sm/La mantle component. Arc and MORB fields after Plank (2005). Average E-MORB and N-MORB compositions after Sun & McDonough (1989).

Figure 12. Schematic model for the development of the Fiordland sector of the Gondwana margin from the Triassic to Early Cretaceous. a) Arc-related magmatism in the outboard arc (Darran Suite) from ca. 230 to 136 Ma. Magmatism is characterized by low-Sr/Y plutons with depleted mantle radiogenic isotope values. b) Development of a ‘tear’ or ridge-trench collision after ca. 136 Ma results in opening of a slab window and upwelling of asthenospheric mantle. High-Sr/Y melts are generated from ① partial melting of subducted, eclogite-facies sedimentary rocks and oceanic crust. Subsequent hybridization occurs by ② mixing of high-Sr/Y melts with a) metasomatized subcontinental mantle lithosphere, and/or b) basaltic melts derived from partial melting of the same mantle lithosphere. c) Peak high-MAR event occurs as upwelling asthenospheric mantle continues to melt subducted, eclogite-facies oceanic crust and impinges on hydrous subcontinental lithospheric mantle igniting the Cretaceous flare up. d) Waning high-Sr/Y magmatism, and granulite- to amphibolite-facies metamorphism in the lower to middle crust (Stowell et al. 2014). Decompression in the lower crust initiates at ca. 108-106 Ma during regional extension and A-type magmatism (Tulloch et al., 2009; Klepeis et al.,

2016; Schwartz et al., 2016). Possible foundering of thick ultramafic root produced during high-Sr/Y flare-up event.

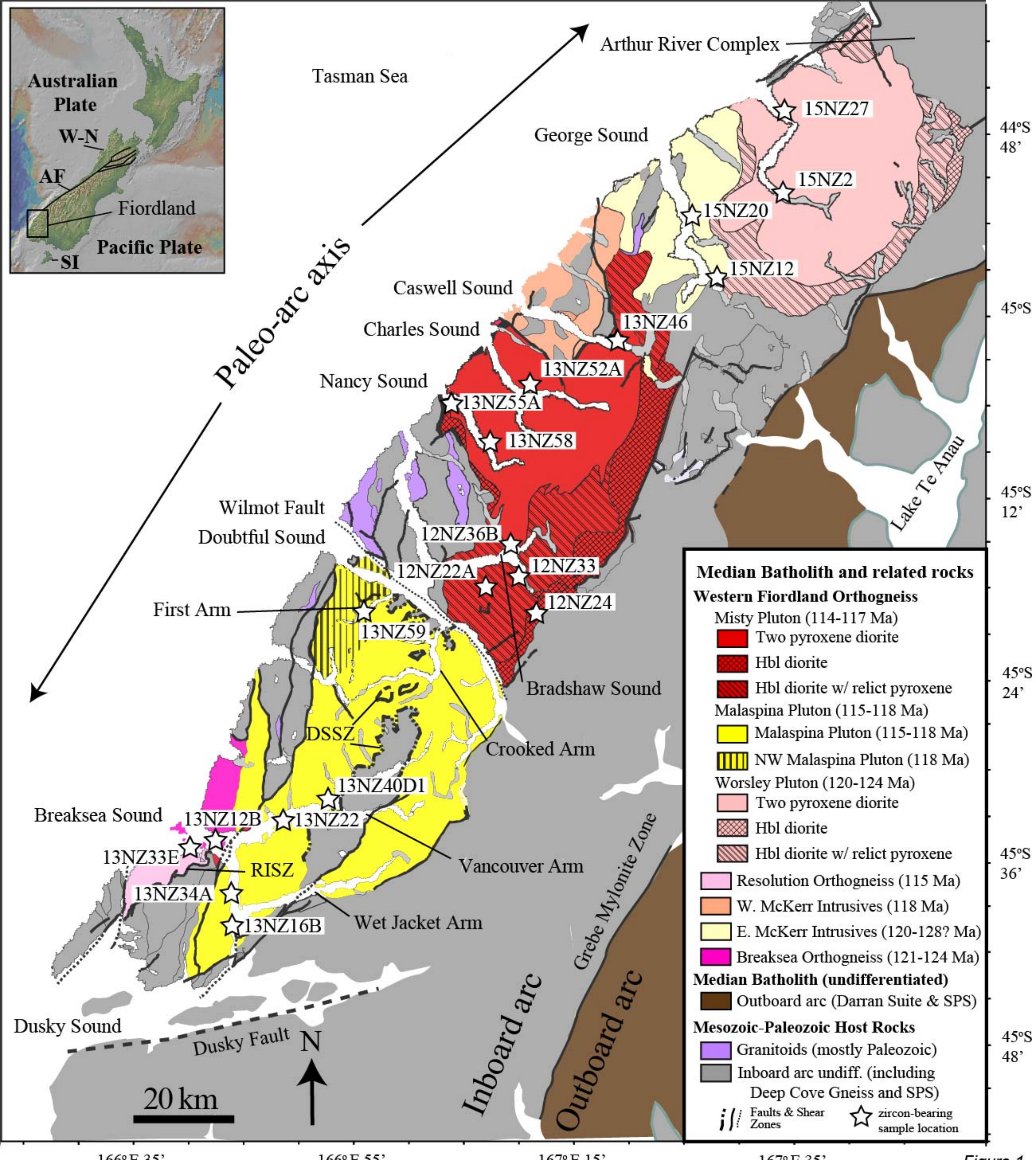
Australian Plate
W-N
AF
Fiordland
Pacific Plate
SI
Tasman Sea
Arthur River Complex
Paleo-arc axis
George Sound
15NZ27
15NZ2
15NZ20
15NZ12
Caswell Sound
Charles Sound
13NZ46
Nancy Sound
13NZ52A
13NZ55A
13NZ58
Wilmot Fault
Doubtful Sound
12NZ36B
12NZ22A
12NZ33
12NZ24
First Arm
13NZ59
Bradshaw Sound
DSSZ
Crooked Arm
13NZ40D1
Breaksea Sound
13NZ12B
13NZ22
13NZ33E
RISZ
Vancouver Arm
13NZ34A
13NZ16B
Wet Jacket Arm
Grebe Mylonite Zone
Lake Te Anau
Dusky Sound
Dusky Fault
N
20 km
Inboard arc
Outboard arc
44°S 48'
45°S
45°S 12'
45°S 24'
45°S 36'
45°S 48'
166° E 35'
166° E 55'
167° E 15'
167° E 35'
Median Batholith and related rocks
Western Fiordland Orthogneiss
Misty Pluton (114-117 Ma)
Two pyroxene diorite
Hbl diorite
Hbl diorite w/ relict pyroxene
Malaspina Pluton (115-118 Ma)
Malaspina Pluton (115-118 Ma)
NW Malaspina Pluton (118 Ma)
Worsley Pluton (120-124 Ma)
Two pyroxene diorite
Hbl diorite
Hbl diorite w/ relict pyroxene
Resolution Orthogneiss (115 Ma)
W. McKerr Intrusives (118 Ma)
E. McKerr Intrusives (120-128? Ma)
Breaksea Orthogneiss (121-124 Ma)
Median Batholith (undifferentiated)
Outboard arc (Darran Suite & SPS)
Mesozoic-Paleozoic Host Rocks
Granitoids (mostly Paleozoic)
Inboard arc undiff. (including Deep Cove Gneiss and SPS)
Faults & Shear Zones
zircon-bearing sample location

Figure 1

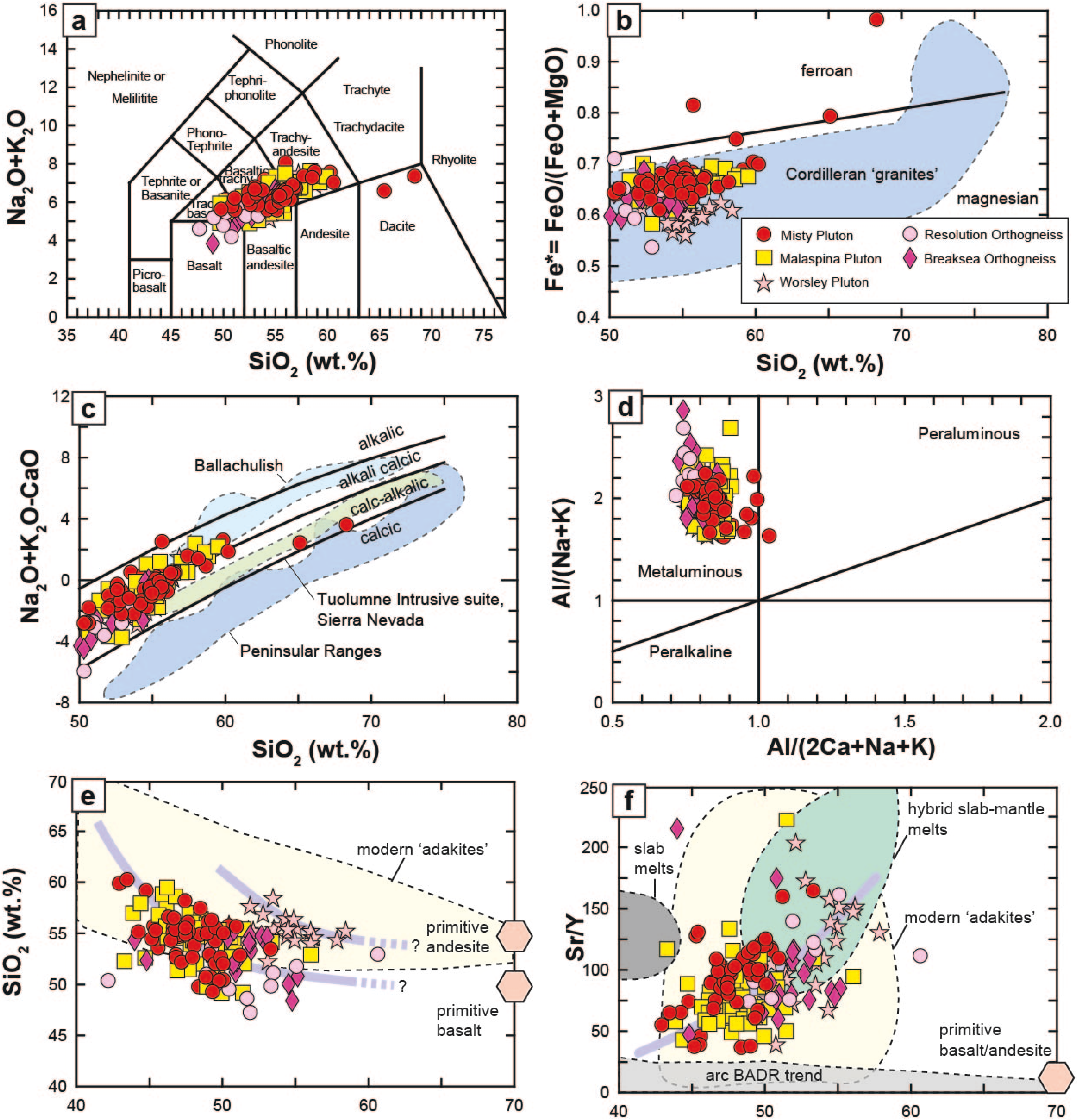
a
b
c
d
e
f
Na2O+K2O
SiO2 (wt.%)
Phonolite
Nephelinite or Melilitite
Tephri-phonolite
Trachyte
Phono-Tephrite
Trachy-andesite
Trachydacite
Rhyolite
Tephrite or Basanite
Basaltic
Basalt
Basaltic andesite
Andesite
Dacite
Picro-basalt
Fe*= FeO/(FeO+MgO)
ferroan
magnesian
Cordilleran 'granites'
Misty Pluton
Malaspina Pluton
Worsley Pluton
Resolution Orthogneiss
Breaksea Orthogneiss
Na2O+K2O-CaO
alkalic
alkali calcic
calc-alkalic
calcic
Ballachulish
Tuolumne Intrusive suite, Sierra Nevada
Peninsular Ranges
Al/(Na+K)
Al/(2Ca+Na+K)
Peraluminous
Metaluminous
Peralkaline
SiO2 (wt.%)
molar Mg#
modern 'adakites'
primitive andesite
primitive basalt
Sr/Y
slab melts
hybrid slab-mantle melts
primitive basalt/andesite
arc BADR trend

Figure 2

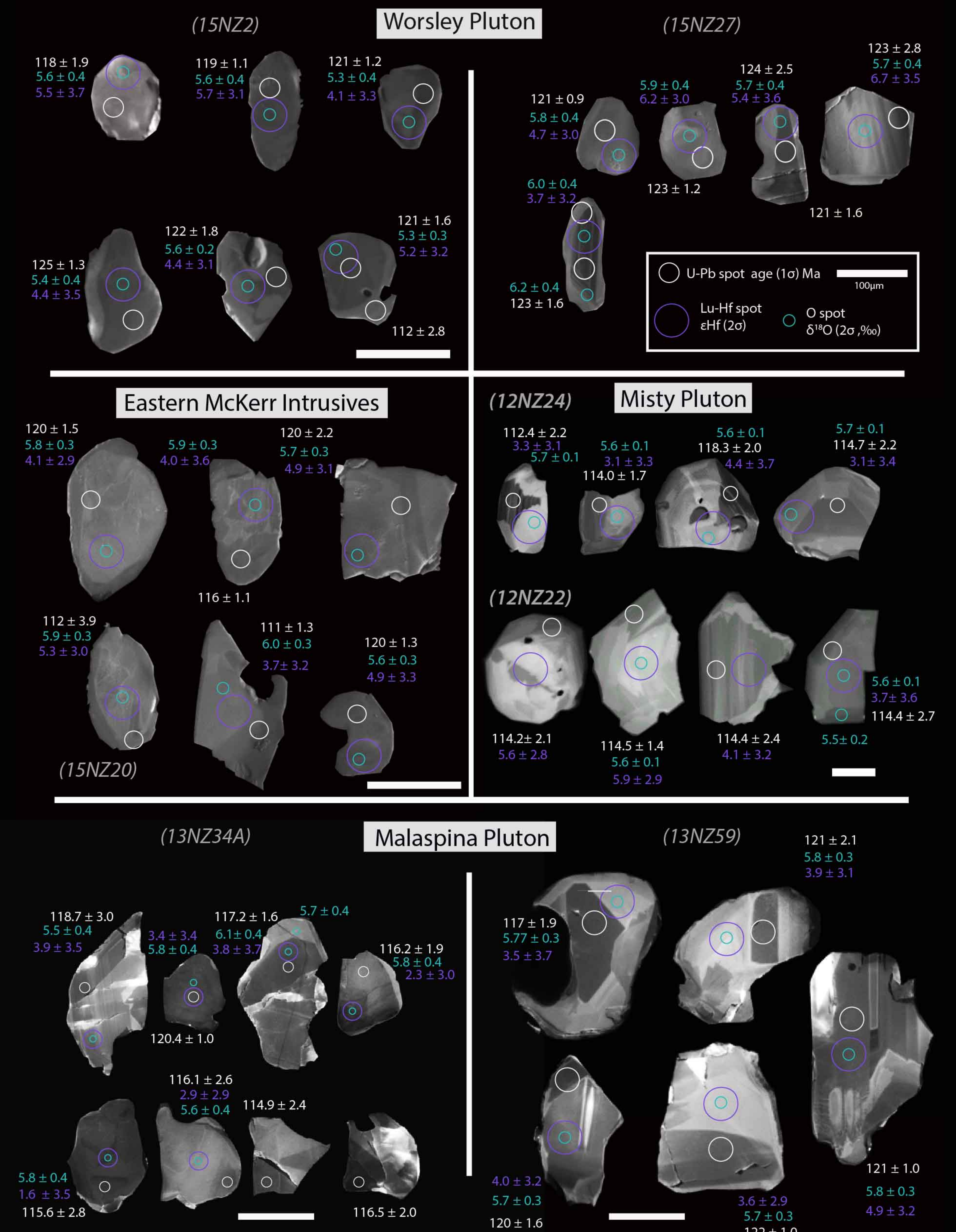

Worsley Pluton
(15NZ2)
(15NZ27)
118 ± 1.9
5.6 ± 0.4
5.5 ± 3.7
119 ± 1.1
5.6 ± 0.4
5.7 ± 3.1
121 ± 1.2
5.3 ± 0.4
4.1 ± 3.3
121 ± 0.9
5.8 ± 0.4
4.7 ± 3.0
5.9 ± 0.4
6.2 ± 3.0
123 ± 1.2
124 ± 2.5
5.7 ± 0.4
5.4 ± 3.6
123 ± 2.8
5.7 ± 0.4
6.7 ± 3.5
121 ± 1.6
6.0 ± 0.4
3.7 ± 3.2
6.2 ± 0.4
123 ± 1.6
125 ± 1.3
5.4 ± 0.4
4.4 ± 3.5
122 ± 1.8
5.6 ± 0.2
4.4 ± 3.1
121 ± 1.6
5.3 ± 0.3
5.2 ± 3.2
112 ± 2.8
U-Pb spot age (1σ) Ma
100μm
Lu-Hf spot εHf (2σ)
O spot δ18O (2σ ,‰)
Eastern McKerr Intrusives
120 ± 1.5
5.8 ± 0.3
4.1 ± 2.9
5.9 ± 0.3
4.0 ± 3.6
116 ± 1.1
120 ± 2.2
5.7 ± 0.3
4.9 ± 3.1
112 ± 3.9
5.9 ± 0.3
5.3 ± 3.0
111 ± 1.3
6.0 ± 0.3
3.7± 3.2
120 ± 1.3
5.6 ± 0.3
4.9 ± 3.3
(15NZ20)
Misty Pluton
(12NZ24)
112.4 ± 2.2
3.3 ± 3.1
5.7 ± 0.1
5.6 ± 0.1
3.1 ± 3.3
114.0 ± 1.7
5.6 ± 0.1
118.3 ± 2.0
4.4 ± 3.7
5.7 ± 0.1
114.7 ± 2.2
3.1± 3.4
(12NZ22)
114.2± 2.1
5.6 ± 2.8
114.5 ± 1.4
5.6 ± 0.1
5.9 ± 2.9
114.4 ± 2.4
4.1 ± 3.2
5.6 ± 0.1
3.7± 3.6
114.4 ± 2.7
5.5± 0.2
Malaspina Pluton
(13NZ34A)
(13NZ59)
118.7 ± 3.0
5.5 ± 0.4
3.9 ± 3.5
3.4 ± 3.4
5.8 ± 0.4
120.4 ± 1.0
117.2 ± 1.6
6.1± 0.4
3.8 ± 3.7
5.7 ± 0.4
116.2 ± 1.9
5.8 ± 0.4
2.3 ± 3.0
116.1 ± 2.6
2.9 ± 2.9
5.6 ± 0.4
114.9 ± 2.4
5.8 ± 0.4
1.6 ± 3.5
115.6 ± 2.8
116.5 ± 2.0
117 ± 1.9
5.77 ± 0.3
3.5 ± 3.7
121 ± 2.1
5.8 ± 0.3
3.9 ± 3.1
4.0 ± 3.2
5.7 ± 0.3
120 ± 1.6
3.6 ± 2.9
5.7 ± 0.3
122 ± 1.0
121 ± 1.0
5.8 ± 0.3
4.9 ± 3.2

Figure 3

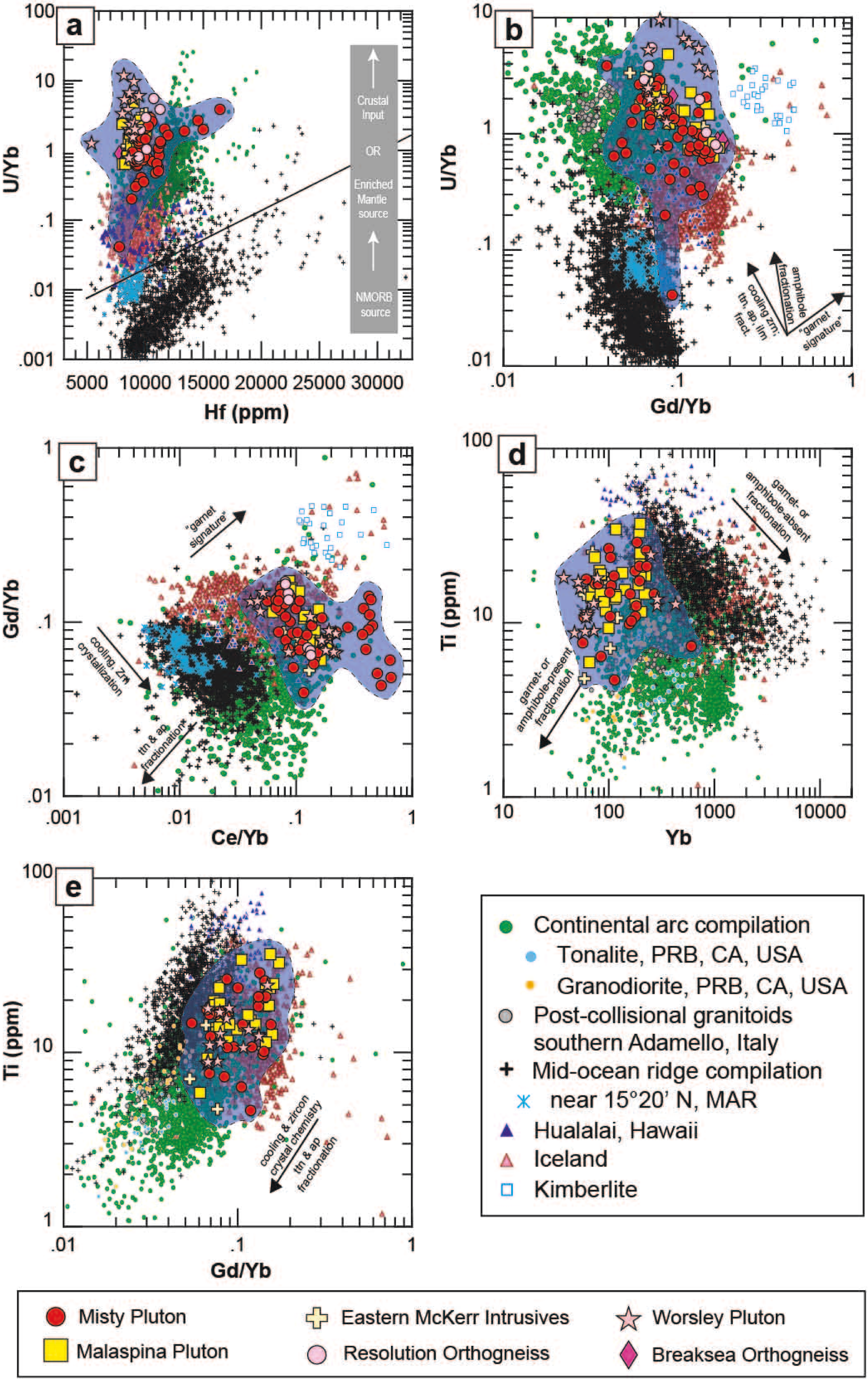
a
U/Yb
Hf (ppm)
Crustal Input
OR
Enriched Mantle source
NMORB source
b
U/Yb
Gd/Yb
amphibole fractionation
cooling zrn; ttn, ap, ilm fract.
"garnet signature"
c
Gd/Yb
Ce/Yb
"garnet signature"
cooling, Zrn crystallization
ttn & ap fractionation
d
Ti (ppm)
Yb
garnet- or amphibole-absent fractionation
garnet- or amphibole-present fractionation
e
Ti (ppm)
Gd/Yb
cooling & zircon crystal chemistry
ttn & ap fractionation
Continental arc compilation
Tonalite, PRB, CA, USA
Granodiorite, PRB, CA, USA
Post-collisional granitoids southern Adamello, Italy
Mid-ocean ridge compilation
near 15°20' N, MAR
Hualalai, Hawaii
Iceland
Kimberlite
Misty Pluton
Malaspina Pluton
Eastern McKerr Intrusives
Resolution Orthogneiss
Worsley Pluton
Breaksea Orthogneiss

Figure 4

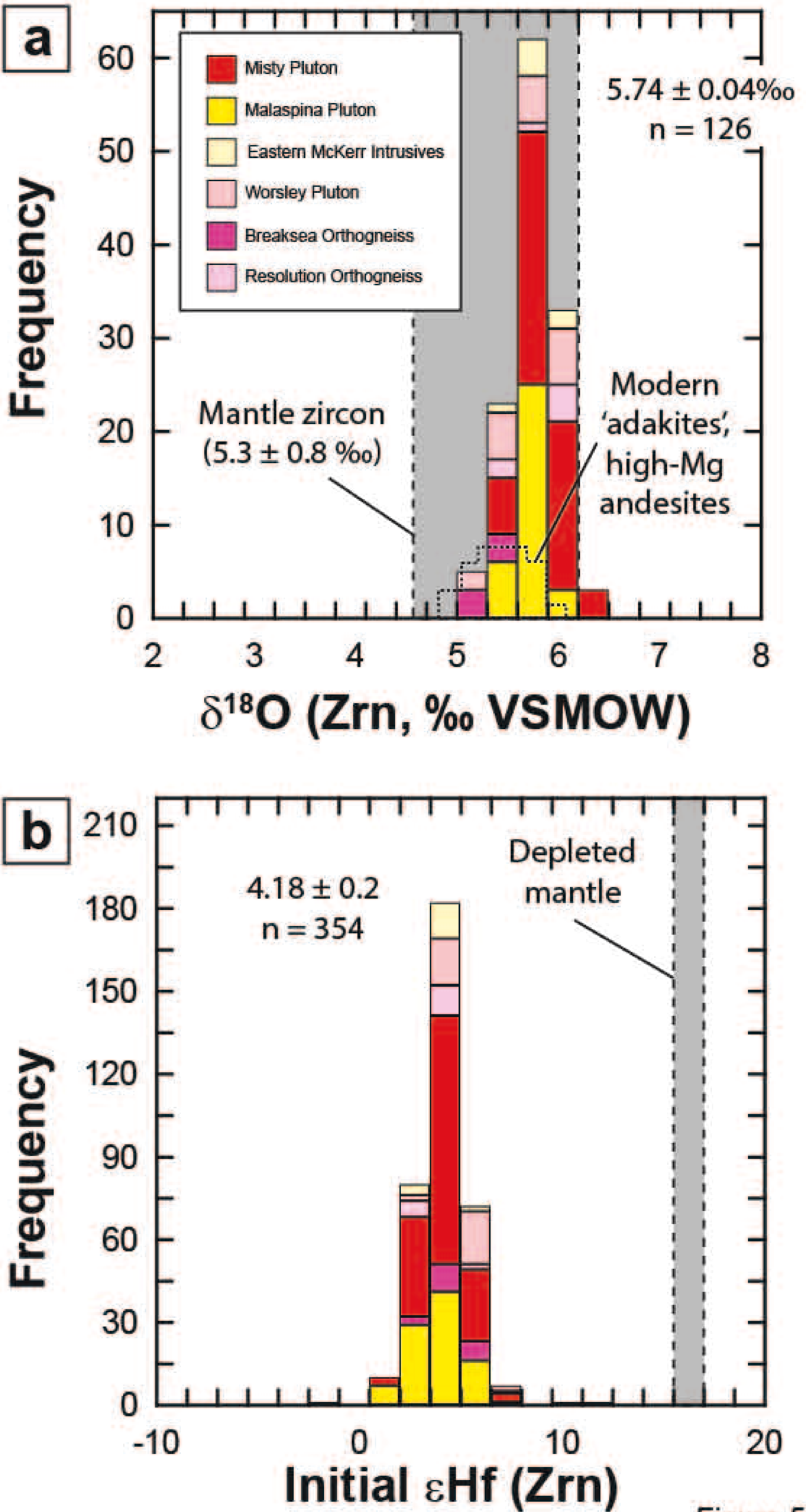

a
Misty Pluton
Malaspina Pluton
Eastern McKerr Intrusives
Worsley Pluton
Breaksea Orthogneiss
Resolution Orthogneiss
5.74 ± 0.04‰
n = 126
Mantle zircon
(5.3 ± 0.8 ‰)
Modern
'adakites',
high-Mg
andesites
Frequency
0
10
20
30
40
50
60
2
3
4
5
6
7
8
δ18O (Zrn, ‰ VSMOW)
b
4.18 ± 0.2
n = 354
Depleted
mantle
Frequency
0
30
60
90
120
150
180
210
-10
0
10
20
Initial εHf (Zrn)

Figure 5

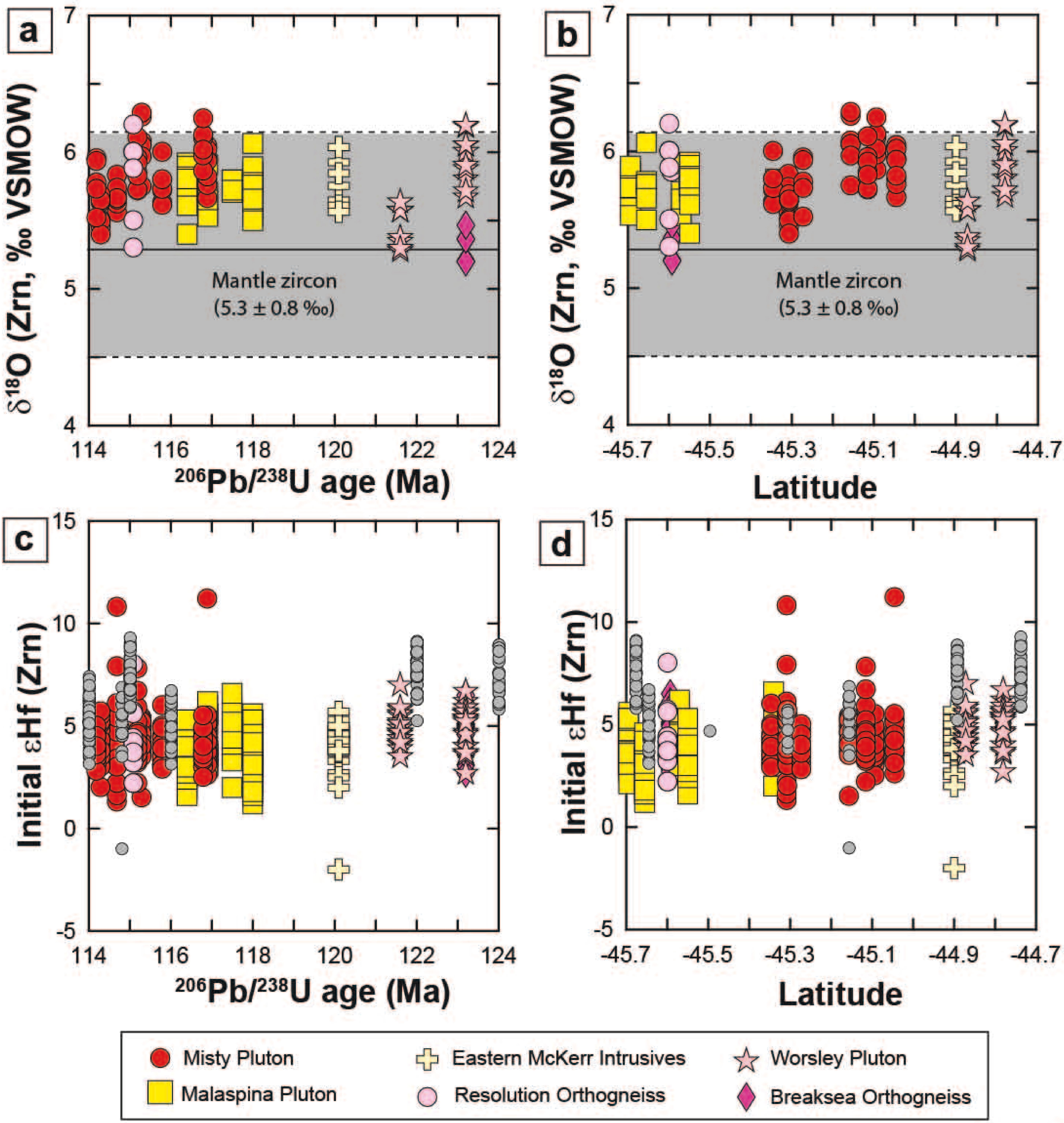

a
b
c
d
δ18O (Zrn, ‰ VSMOW)
Initial εHf (Zrn)
206Pb/238U age (Ma)
Latitude
Mantle zircon
(5.3 ± 0.8 ‰)
Misty Pluton
Malaspina Pluton
Eastern McKerr Intrusives
Resolution Orthogneiss
Worsley Pluton
Breaksea Orthogneiss

Figure 6

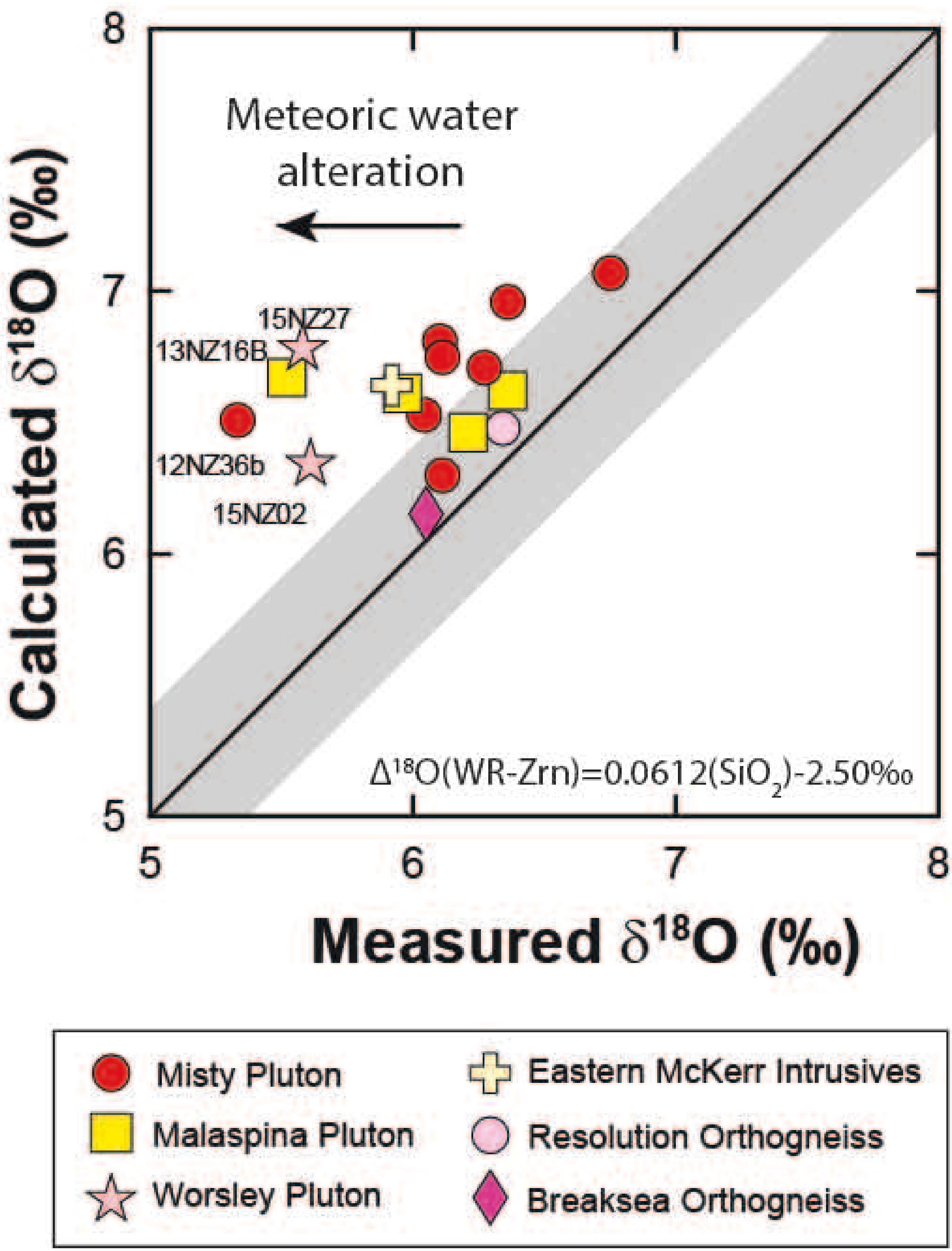

8
7
6
5
Calculated δ18O (‰)
Meteoric water
alteration
15NZ27
13NZ16B
12NZ36b
15NZ02
Δ18O(WR-Zrn)=0.0612(SiO2)-2.50‰
5
6
7
8
Measured δ18O (‰)
Misty Pluton
Malaspina Pluton
Worsley Pluton
Eastern McKerr Intrusives
Resolution Orthogneiss
Breaksea Orthogneiss

Figure 7

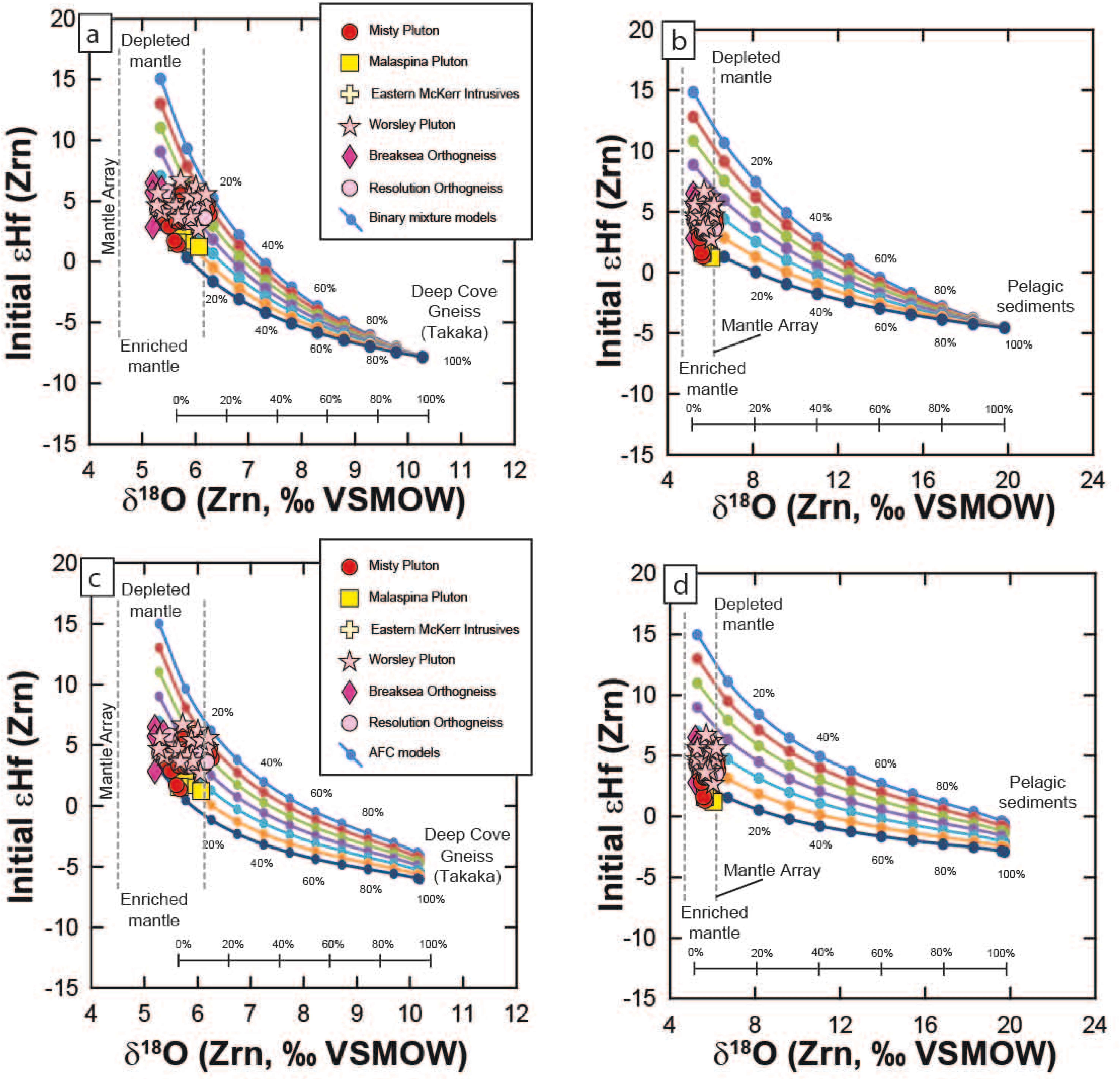
a
b
c
d
Misty Pluton
Malaspina Pluton
Eastern McKerr Intrusives
Worsley Pluton
Breaksea Orthogneiss
Resolution Orthogneiss
Binary mixture models
AFC models
Depleted mantle
Enriched mantle
Mantle Array
Deep Cove Gneiss (Takaka)
Pelagic sediments
Initial εHf (Zrn)
δ18O (Zrn, ‰ VSMOW)
0%
20%
40%
60%
80%
100%

Figure 8

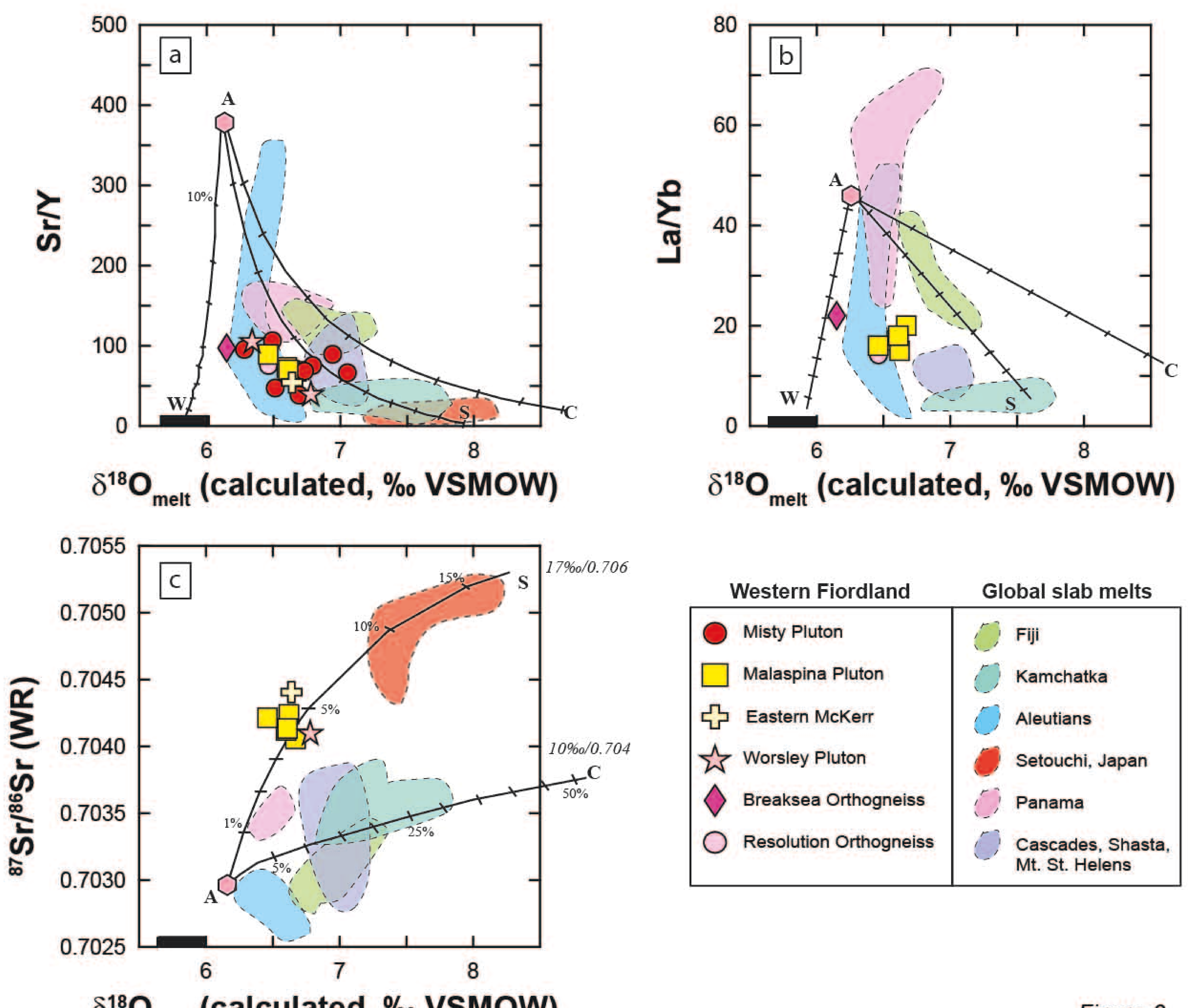
a
Sr/Y
500
400
300
200
100
0
A
W
S
C
10%
6
7
8
δ18Omelt (calculated, ‰ VSMOW)
b
La/Yb
80
60
40
20
0
A
W
S
C
6
7
8
δ18Omelt (calculated, ‰ VSMOW)
c
87Sr/86Sr (WR)
0.7055
0.7050
0.7045
0.7040
0.7035
0.7030
0.7025
17‰/0.706
S
15%
10%
5%
1%
A
5%
25%
50%
10‰/0.704
C
6
7
8
δ18Omelt (calculated, ‰ VSMOW)
Western Fiordland
Misty Pluton
Malaspina Pluton
Eastern McKerr
Worsley Pluton
Breaksea Orthogneiss
Resolution Orthogneiss
Global slab melts
Fiji
Kamchatka
Aleutians
Setouchi, Japan
Panama
Cascades, Shasta, Mt. St. Helens

Figure 9

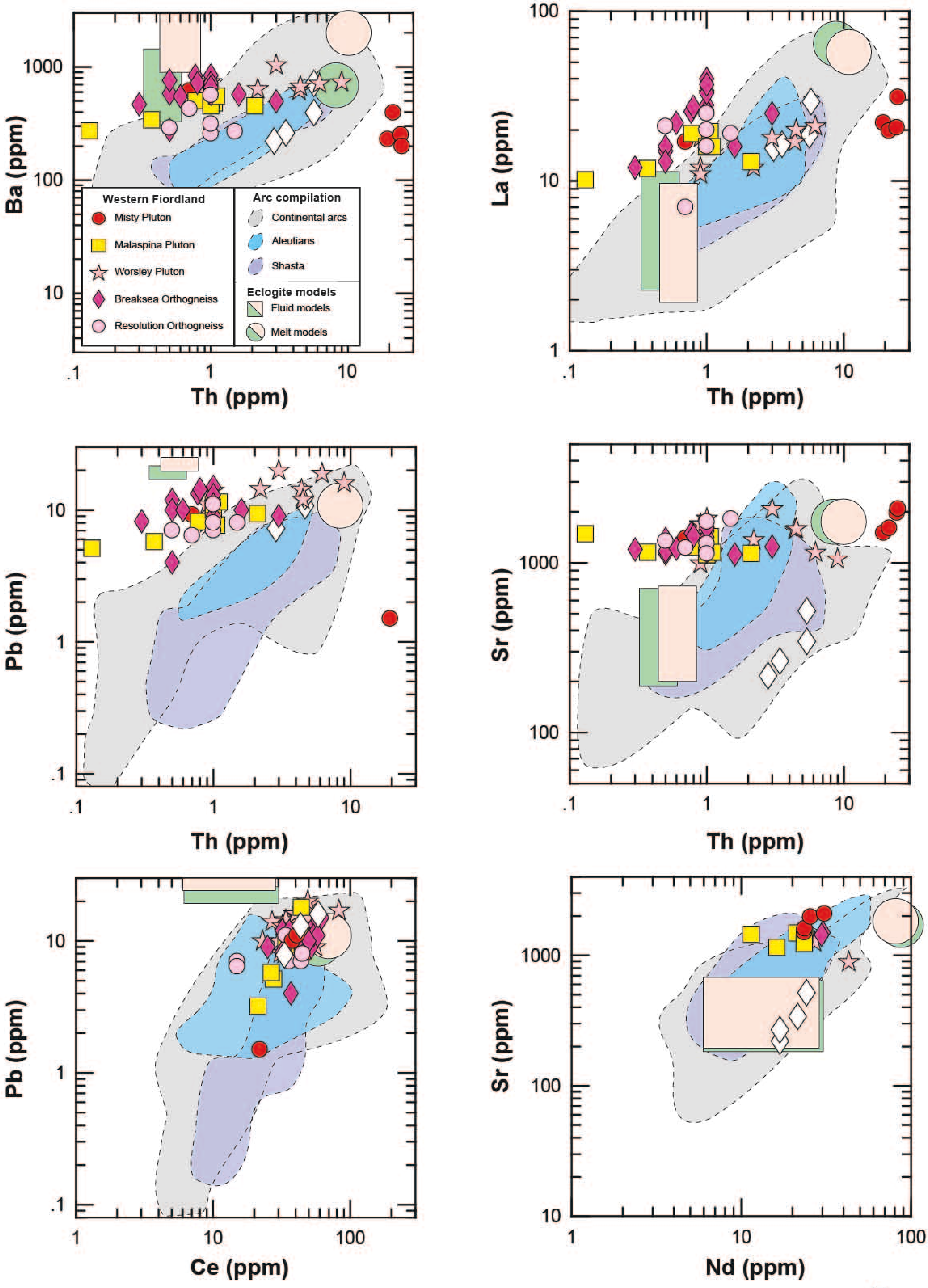

Ba (ppm)
Th (ppm)
Western Fiordland
Misty Pluton
Malaspina Pluton
Worsley Pluton
Breaksea Orthogneiss
Resolution Orthogneiss
Arc compilation
Continental arcs
Aleutians
Shasta
Eclogite models
Fluid models
Melt models
La (ppm)
Th (ppm)
Pb (ppm)
Th (ppm)
Sr (ppm)
Th (ppm)
Pb (ppm)
Ce (ppm)
Sr (ppm)
Nd (ppm)

Figure 10

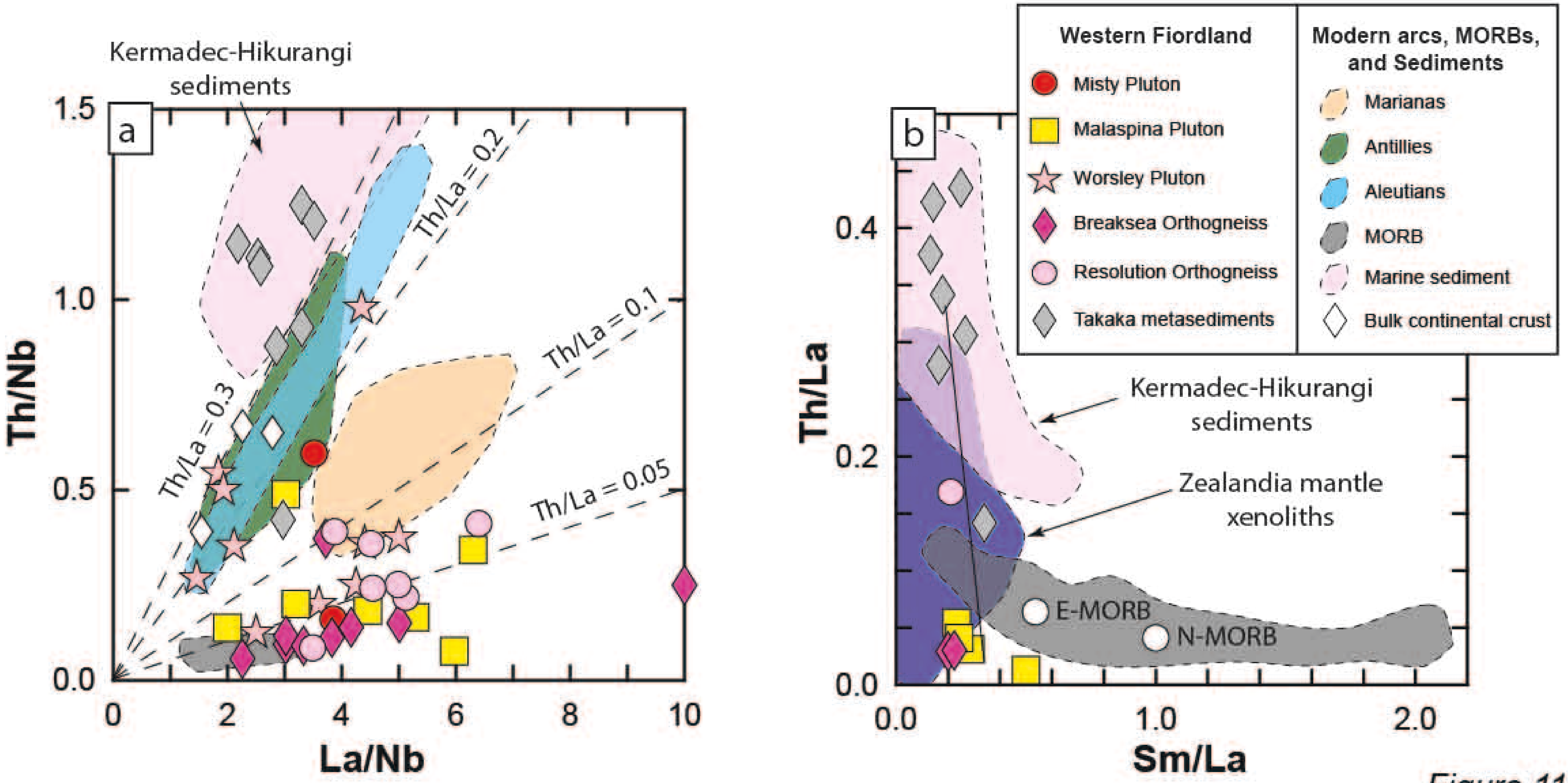

a
Kermadec-Hikurangi sediments
Th/La = 0.3
Th/La = 0.2
Th/La = 0.1
Th/La = 0.05
Th/Nb
La/Nb
0.0
0.5
1.0
1.5
0
2
4
6
8
10
b
Th/La
Sm/La
0.0
0.2
0.4
0.0
1.0
2.0
Kermadec-Hikurangi sediments
Zealandia mantle xenoliths
E-MORB
N-MORB
Western Fiordland
Misty Pluton
Malaspina Pluton
Worsley Pluton
Breaksea Orthogneiss
Resolution Orthogneiss
Takaka metasediments
Modern arcs, MORBs, and Sediments
Marianas
Antillies
Aleutians
MORB
Marine sediment
Bulk continental crust

Figure 11

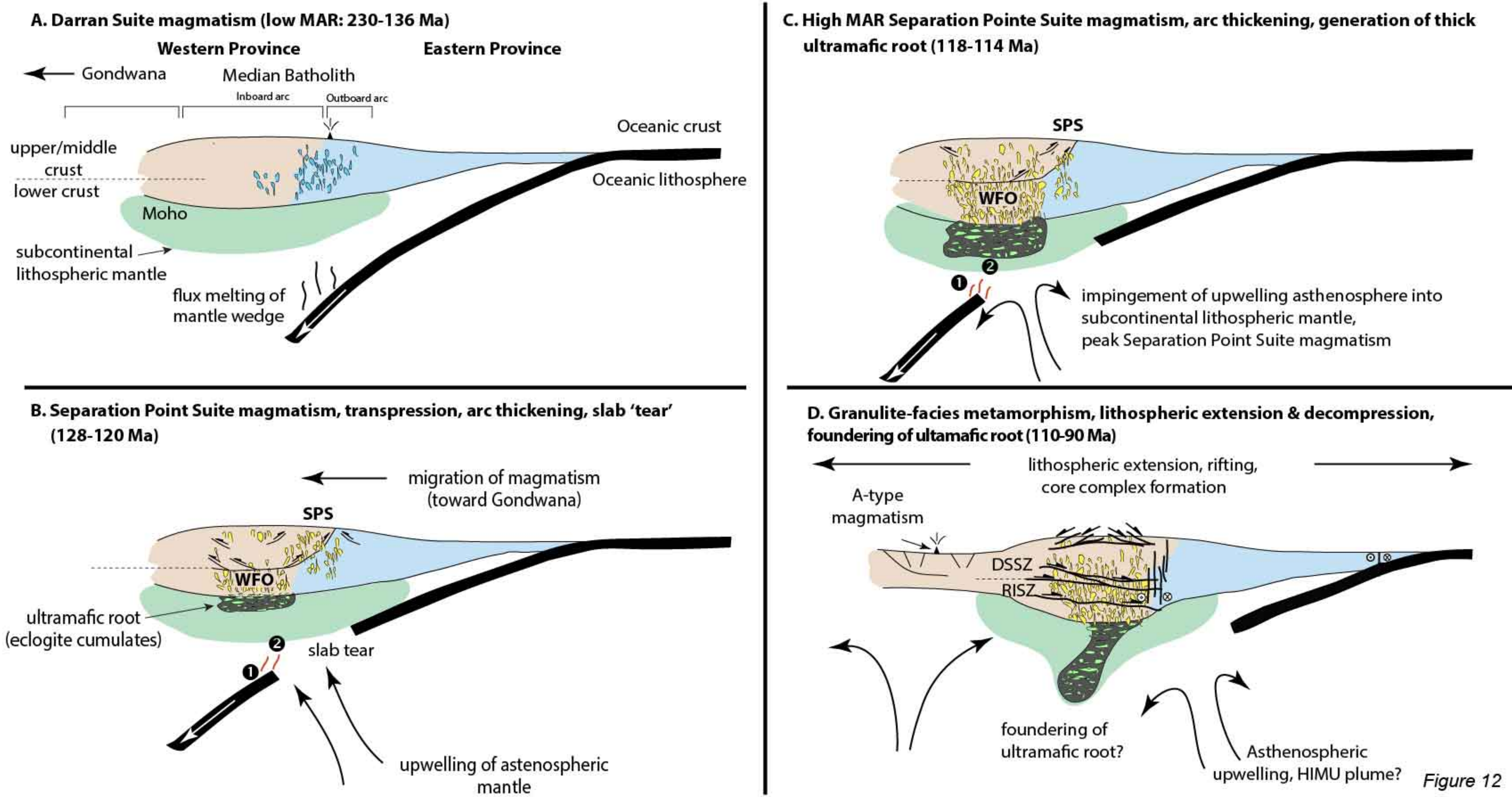

A. Darran Suite magmatism (low MAR: 230-136 Ma)
Western Province
Eastern Province
Gondwana
Median Batholith
Inboard arc
Outboard arc
Oceanic crust
upper/middle crust
lower crust
Oceanic lithosphere
Moho
subcontinental lithospheric mantle
flux melting of mantle wedge
B. Separation Point Suite magmatism, transpression, arc thickening, slab 'tear' (128-120 Ma)
migration of magmatism (toward Gondwana)
SPS
WFO
ultramafic root (eclogite cumulates)
slab tear
upwelling of astenospheric mantle
C. High MAR Separation Pointe Suite magmatism, arc thickening, generation of thick ultramafic root (118-114 Ma)
SPS
WFO
impingement of upwelling asthenosphere into subcontinental lithospheric mantle, peak Separation Point Suite magmatism
D. Granulite-facies metamorphism, lithospheric extension & decompression, foundering of ultamafic root (110-90 Ma)
lithospheric extension, rifting, core complex formation
A-type magmatism
DSSZ
RISZ
foundering of ultramafic root?
Asthenospheric upwelling, HIMU plume?

Figure 12

Table 1. Summary of Zircon U-Pb, O and Lu-Hf isotopic data for the WFO.

Pluton	Rock type	Field sample number	P-Number	Pb/U Zrn Age (Ma) (2E)[!]	SiO_2 (WR)	$\delta^{18}O$ (WR) (‰)	$\delta^{18}O$ (WR) (‰)[!!]	Zrn $\delta^{18}O$ range (‰)	$\delta^{18}O$ (Zrn) mean (‰)	Error (2D)	#	Zrn εHf (initial) range	Zrn εHf (initial) mean	2 SD	#	Ti-in-Zircon temperature (°C)	SD
Breaksea	Gnt granulite	13NZ33E		123.2 ± 1.3	54.7	6.05	6.15	5.2-5.4	5.30	0.23	6	2.7-6.5	4.8	3.5	20	n.d.	n.d.
Eastern McKerr	Hbl diorite	15NZ20	P85715	120.1 ± 2.8	55.1	5.92	6.64	5.5-6.0	5.77	0.27	6	(-) 2.0 - 5.7	3.8	3.1	20	777	57
Malaspina	Hbl diorite	13NZ16B	P83712	118.0 ± 2.1	56.0	5.52	6.67	5.5-5.9	5.74	0.27	7	2.1-5.6	4.2	3.1	20	776	43
Malaspina	Hbl diorite	13NZ22	P83718	116.9 ± 1.6	56.1	4.53	6.60	5.5-5.9	5.67	0.37	5	3.0-6.2	4.3	3.4	17	812	31
Malaspina	Two pyroxene diorite	13NZ34A	P83730	118.0 ± 1.8	55.2	6.36	6.62	5.5-6.0	5.74	0.39	7	1.2-4.6	2.9	3.3	20	792	31
Malaspina	Bt-Hbl diorite with relict pyroxene	13NZ40D1	P83733	116.4 ± 1.3	52.6	6.21	6.46	5.4-5.9	5.74	0.37	9	1.9-5.3	3.6	3.3	17	780	31
Malaspina	Hbl-Bt qz diorite	13NZ59	P83750	117.5 ± 1.0	54.9	5.96	6.61	5.7-5.8	5.75	0.27	6	1.9-6.5	4.3	3.1	20	788	29
Misty	Hbl diorite	12NZ22a	P83650	114.7 ± 1.1	59.2	6.11	6.80	5.5-5.8	5.68	0.17	7	1.3-10.8	4.7	3.4	20	n.d.	n.d.
Misty	Hbl diorite	12NZ24	P83652	115.8 ± 2.1	53.5	6.05	6.52	5.6-6.0	5.75	0.12	6	2.9-6.0	3.9	3.3	20	n.d.	n.d.
Misty	Hbl monzodiorite	12NZ33	P83661	114.3 ± 2.1	52.9	6.12	6.29	5.4-5.6	5.56	0.23	8	2.0-5.7	4.0	3.6	20	n.d.	n.d.
Misty	Bt-Hbl qz diorite with relict pyroxene	12NZ36b	P83664	114.2 ± 1.3	52.6	5.34	6.50	5.5-5.9	5.78	0.20	5	2.8-4.9	3.9	3.4	20	n.d.	n.d.
Misty	Two pyroxene monzodiorite	13NZ46	P83738	116.9 ± 1.2	54.5	6.28	6.70	5.6-6.0	5.87	0.17	8	2.6-11.2	4.4	3.1	20	795	21
Misty	Two pyroxene diorite	13NZ52A	P83743	116.8 ± 1.6	55.5	6.37	6.95	5.8-6.2	6.05	0.38	5	2.5-5.4	3.9	2.9	20	776	26
Misty	Hbl-Bt qz diorite	13NZ55A	P83746	115.2 ± 1.9	60.2	6.76	7.06	5.7-6.1	5.87	0.40	7	2.1-7.7	4.4	2.9	20	773	48
Misty	Two pyroxene diorite	13NZ58	P83749	115.3 ± 1.5	52.0	6.12	6.74	5.7-6.2	6.06	0.27	7	1.4-5.4	4.3	2.9	20	735	32
Resolution	Hbl diorite	12NZ12b		115.1 ± 2.1	51.0	6.35	6.47	5.3-6.1	5.85	0.25	7	2.2-7.9	4.0	3.2	20	n.d.	n.d.
Worsley	Two pyroxene diorite	15NZ02	P85716	121.6 ± 1.9	55.3	5.61	6.34	5.2-5.6	5.46	0.38	8	3.5-6.9	4.9	3.3	20	745	17
Worsley	Two pyroxene diorite	15NZ27	P85717	123.2 ± 1.6	54.4	5.58	6.78	5.6-6.2	5.95	0.45	10	2.6-6.1	5.0	3.1	20	781	24

[!]U-Pb zircon data reported in Schwartz et al. (in press), except 13NZ33E which is reported in Klepeis et al. (2016).

[!!]calculated using equation reported in Lackey et al. (2008).

SE = standard error; SD = Standard deviation; n.d. = not determined.